

# Optimization of bend test set up to quantify effect of surface roughness on fatigue properties

*A guideline to four-point bending and how to optimize specimen geometry.*

Sebastian Issa

24 March 2026

Master's Thesis

## **Examiner**

Zuheir Barsoum

## **Academic adviser**

Zuheir Barsoum

## **Industrial adviser**

Tobias Mattsson



## Abstract

Mechanical testing is a crucial part of engineering; it reassures safety in products, which is of utmost importance in the Aerospace industry. Additive manufacturing, AM, is being used more widely in this sector, and a common testing method for components with AM surfaces is four-point bending. This method is in theory great for investigating and determining the influence surface roughness has on fatigue life properties, but there are many uncertainties which compromise the validity of 4PB.

This thesis project explores some of these uncertainties and attempts to increase the validity of four-point bending. The specimen geometry is one of the major points of research in this project. It explores how the design of the specimen can be optimized to minimize an inherent error of 4PB: wedging stress. This thesis also explores how sensitive four-point bending is to setup errors, specifically eccentric- and non-perpendicular-loading. The project is based on FEA simulations performed in Ansys Workbench.

The wedging error was proven to be less severe than it was thought to be at the beginning of the project. The baseline specimen, which was based on a common specimen used at GKN Aerospace, showed localized stress peaks that were 1.37% larger than nominal stress. Which is within the total error limit of  $\pm 5\%$ . Furthermore, this could be further minimized by increasing the difference between the inner and outer rollers. It was also found that if the inner roller distance is smaller than three tenths of the outer roller distance, the test transitioned towards pseudo-3PB behavior. Consequently, this method is not suitable for thin and wide specimens, since if the breadth of the specimen became bigger than double the height the error started increasing rapidly.

Four-point bending proved to be more sensitive to eccentric loading and was barely influenced by non-perpendicular loading, at least when it comes to peak stress. Additionally, it was discovered that 4PB is less sensitive to eccentric loading when the inner rollers are applying the load.

### Keywords

Four-Point Bending (4PB), Mechanical Testing, Bend Testing, Fatigue, Additive Manufacturing (AM), Finite Element Analysis (FEA), Finite Element Method (FEM)



## Sammanfattning

Mekanisk provning är en väsentlig del av produktutvecklingen, eftersom detta säkerställer att produkterna som tillverkas är säkra, vilket är särskilt viktigt inom flyg-och-rymd industrin. Additiv tillverkning, AM, används dessutom mer och mer inom denna industri. En vanlig provmetod som används för att testa produkter med AM ytor är fyr-punkts böj provning. Teoretiskt sätt är metoden enastående för att undersöka och utvärdera hur ytjämnheten påverkar utmattningsegenskaper, men metoden är inte helt fastställd, vilket äventyrar metodens giltighet.

Detta arbete utforskar några av de osäkerheter som drabbar 4PB i ett försök att öka dess giltighet. Provtavsgeometrin är ett av huvudområdena, utformningen av provstaven har undersökts huruvida denna kan optimeras för att minimera ett fel som alltid uppstår vid fyr-punkts böj: kilning. Arbetet utforskar även hur känsligt 4PB är gentemot fel i själva provmaskinen, specifikt excenterapplicerad last och last som inte är applicerad vinkelrät mot provstavens yta. Arbetet är baserat på FEM simuleringar i Ansys Workbench.

Det framkom att kilningsfelet inte var lika allvarligt som det antogs vara vid början av arbetet. Den provtavsgeometrin som användes som baslinje för arbetet, vilken var baserad på en vanlig provtavsgeometri som används på GKN Aerospace, visades sig ha lokala spänningsmaxima som enbart var 1.37% högre än den nominella spänningen. Vilket ligger väl inom den totala felmarginalen på  $\pm 5\%$ . Dessutom kunde felet minimeras genom att öka skillnaden mellan ytter-och inner-rullarnas avstånd. Vidare upptäcktes det att om avståndet mellan innerrullarna var mindre än tre tiondelar av ytterrullarnas avstånd började provet röra sig mot ett pseudo-3PB beteende. Utöver detta upptäcktes det att metoden inte är lämpad för tunna och breda provstavar. När provstaven är dubbelt så bred som den är hög ökar spänningsfelet hastigt.

Fyr-punkts böj har visat sig vara känsligare för excentriskt placerade laster än för icke-vinkelräta laster, åtminstone när det gäller lokala spänningsmaxima. En ytterligare upptäckt var att känsligheten för excentriskt placerade laster minskar när innerrullarna applicerar lasten.

### Nyckelord

Fyr-Punkts Böj (4PB), Mekanisk Provning, Böj Provning, Utmattning, Additiv Tillverkning (AM), Finit Element Analys, Finita Elementmetoden (FEM)



## Acknowledgments

I would like to start by thank GKN Aerospace for giving me the opportunity to write my master's thesis at their premises in my hometown, Trollhättan. It has been an incredible journey, and it undoubtedly helped that I was surrounded by the incredible group of people at the mechanical testing department, their continuous support and interest kept the thesis going and kept me motivated.

I would like to specifically thank my supervisor at GKN, Tobias Mattsson. Without his supervision, this thesis project would not have been possible.

I want to extend this gratitude to my academic supervisor, Professor Zuheir Barsoum. It was thanks to his encouragement that I applied to write this thesis and his involvement in the thesis kept me on track.

I would also like to thank my mentors, Dr. Thomas Hansson and Jonas Kullgren. They provided me with two different sides of the thesis: pure theoretical and practical application respectively. Thomas also acted as a conduit between academic and industrial aspects of the project and was the one who got me in contact with Tobias.

I would like to thank the solid mechanics researchers at University West who have shown an interest in my thesis and provided me with valuable insight when presenting the unfinished thesis at their premises.

I would also like to thank my friends and family who have been supporting me all the way from start to finish.

And finally, I want to thank KTH for helping me grow as a person and for providing me with the tools and knowledge necessary to accomplish what I have.

Trollhättan, March 2026  
Sebastian Issa



## Table of Contents

<b>Abstract</b> .....	<b>i</b>
<b>Keywords</b> .....	<b>i</b>
<b>Sammanfattning</b> .....	<b>iii</b>
<b>Nyckelord</b> .....	<b>iii</b>
<b>Acknowledgments</b> .....	<b>v</b>
<b>Table of Contents</b> .....	<b>vii</b>
<b>List of Figures</b> .....	<b>ix</b>
<b>List of Tables</b> .....	<b>xi</b>
<b>List of acronyms and abbreviations</b> .....	<b>xiii</b>
<b>1 Introduction</b> .....	<b>1</b>
<b>1.1 Background</b> .....	<b>1</b>
<b>1.2 Problem</b> .....	<b>2</b>
<b>1.3 Purpose</b> .....	<b>2</b>
<b>1.4 Goals</b> .....	<b>2</b>
<b>1.5 Research Methodology</b> .....	<b>3</b>
<b>1.6 Delimitations</b> .....	<b>3</b>
<b>1.7 Structure of the Thesis</b> .....	<b>3</b>
<b>2 Background</b> .....	<b>5</b>
<b>2.1 Literature review</b> .....	<b>5</b>
2.1.1 Oxford article results .....	5
2.1.2 Oxford simulation model .....	7
2.1.3 Oxford article summary.....	7
2.1.4 Alternate geometry.....	8
<b>2.2 Mechanical Testing</b> .....	<b>8</b>
2.2.1 Flexural testing.....	8
2.2.2 Mechanical testing at GKN .....	9
<b>2.3 GKN 4PB Test Setup</b> .....	<b>9</b>
<b>2.4 Summary</b> .....	<b>10</b>
<b>3 Methodology &amp; Implementation</b> .....	<b>11</b>
<b>3.1 Beam Theory Calculations</b> .....	<b>11</b>
<b>3.2 Building the Simulation Model</b> .....	<b>12</b>
<b>3.3 Final Model</b> .....	<b>15</b>
<b>3.4 Model Validation</b> .....	<b>17</b>
<b>3.5 Parameter Study</b> .....	<b>17</b>
3.5.1 Proposed ideal ratios .....	18
3.5.2 Alternate geometry evaluation .....	18
3.5.3 Cross section study.....	19
3.5.4 Roller placement study .....	19
<b>3.6 Error Sensitivity Study</b> .....	<b>19</b>
3.6.1 Eccentric loading.....	19
3.6.2 Non-perpendicular loading.....	21
<b>4 Results and Analysis</b> .....	<b>23</b>
<b>4.1 FEA Model Comparison</b> .....	<b>23</b>
<b>4.2 Model Validity Analysis</b> .....	<b>23</b>
<b>4.3 Parameter Study Results</b> .....	<b>24</b>
4.3.1 Alternate geometry comparison.....	24

4.3.2	Cross section study results .....	25
4.3.3	Roller placement study results.....	27
<b>4.4</b>	<b>Error Sensitivity Result .....</b>	<b>29</b>
4.4.1	Eccentric loading results .....	29
4.4.2	Non-perpendicular loading results .....	33
<b>4.5</b>	<b>Discussion .....</b>	<b>35</b>
<b>5</b>	<b>Conclusions and Future Work .....</b>	<b>37</b>
5.1	Conclusions.....	37
5.2	Limitations .....	37
5.3	Future Work .....	38
5.4	Reflections .....	38
	References .....	39
	Appendix A: 4PB Test Rig at GKN Aerospace.....	41
	Appendix B: Specimen Drawing .....	42
	Appendix C: Geometry Study of a Proposed Ideal Specimen.....	43
	Appendix D: Non-Perpendicular Loading Surfaces .....	44

## List of Figures

Figure 1-1:	Diagram comparing 3PB (left) and 4PB (right), with their corresponding BMD. ....	1
Figure 2-1:	4PB diagram from [4] with the same nomenclature as this thesis. ....	5
Figure 2-2:	FEA results where the maximum stress is plotted against $x/l$ , the normalized inner roller distance. The geometry is varied according to the $l/h$ ratio (left) and $L/l$ ratio (right). ....	5
Figure 2-3:	Surface stress during 4PB testing influenced by wedging. The dotted line is the calculated stress in ideal loading [7]. ....	6
Figure 2-4:	Schematic of FEA model used by [4] with new nomenclature. ....	7
Figure 2-5:	The specimen used by [8] implemented into 4PB fatigue tests of AM surfaces. ....	8
Figure 2-6:	The micro strain gauge placements on the specimen test surface. ....	9
Figure 3-1:	BMD and SFD for a common 4PB specimen, inner rollers are placed at the ends of the horizontal moment line and outer rollers are placed at the ends of the moment curve. ....	11
Figure 3-2:	Diagram of the 4PB method with the nomenclature used in this thesis project. ....	12
Figure 3-3:	The resulting mesh of the recreated 2D model. ....	13
Figure 3-4:	The boundary conditions of the model recreation, test surface is indicated via the pink line. ....	13
Figure 3-5:	Primary comparison between [4] and the FEA model of this thesis. ....	14
Figure 3-6:	Element order comparison (left) and comparison between plane stress and plane strain (right). ....	14
Figure 3-7:	The stress behavior when scoping for different stress types (left) and comparing the behavior in 2D and 3D (right). ....	14
Figure 3-8:	Top view of the baseline 3D model based on a common 4PB specimen. ....	15
Figure 3-9:	The mesh of the 3D model baseline specimen. ....	16
Figure 3-10:	Resulting peak stress behavior when the number of elements, and consequently size, varies. ....	16
Figure 3-11:	Bottom view of the 3D model baseline specimen. The red lines are outer roller contacts, and the pink line is where the stress data is collected. ....	17
Figure 3-12:	Model used for strain verification with the 3 paths marked out and named after the involved channels. ....	17
Figure 3-13:	The normal stress along the test surface for a specimen with dimensions seen in [12] which is based on the ratios stated in [4]. Nominal stress is 600 MPa. ....	18
Figure 3-14:	Diagram of how the parameter $\delta$ is defined. ....	19
Figure 3-15:	Eccentric loading diagram where $\alpha$ is the eccentric offset parameter. ....	19
Figure 3-16:	Eccentric load diagram, when inner rollers are applying the load. ....	20
Figure 3-17:	Eccentric load diagram, when outer rollers are applying the load. ....	20
Figure 3-18:	Diagram of how the inner rollers lines of contact were rotated with a rotational parameter, $\beta$ . ....	21
Figure 3-19:	Diagram of how the outer rollers lines of contact were rotated with a rotational parameter, $\varphi$ . ....	21
Figure 4-1:	Comparison between the attempted recreation and the results presented in [4], for a specimen with $l/h = 3$ . ....	23

Figure 4-2:	Strain deviation of the measured strain compared to the simulated strain at a load of 5 kN. ....	24
Figure 4-3:	The stress comparison between the geometry seen in [8] and a rectangular specimen of the same length and roller placement without the radii: $L_{tot} = 70 \text{ mm}$ , $L = 60 \text{ mm}$ , $l = 20 \text{ mm}$ & a cross section of $6 \times 6 \text{ mm}^2$ .....	24
Figure 4-4:	3D surface plot of the peak stress error in percentage when varying h and b of the baseline specimen with $L = 80 \text{ mm}$ and $l = 40 \text{ mm}$ .....	25
Figure 4-5:	The resulting stress curve when the height is set to 8 mm and the breadth varies.....	26
Figure 4-6:	The resulting stress curves when the height varies and the breadth is set to 4 mm.....	26
Figure 4-7:	The stress curve behavior when $b = 2h$ .....	26
Figure 4-8:	The stress behavior for thin and wide specimen geometries.....	27
Figure 4-9:	3D surface plot that shows how the tensile stress error is dependent on the parameters $\delta$ and $L$ .....	27
Figure 4-10:	The surface stress across $l$ while varying $L$ with a constant $\delta$ .....	28
Figure 4-11:	The peak stress error plotted against an increasing $\delta$ when $L = 80 \text{ mm}$ .....	28
Figure 4-12:	Tensile stress deviation across the test surface during an increasing eccentric offset when the inner rollers are applying a constant force of $F/2$ each. ....	29
Figure 4-13:	BMD &SFD comparison during an eccentric offset of 3 mm when inner rollers are applying the load.....	29
Figure 4-14:	The peak stress deviation in percentage when the eccentric offset increases.....	30
Figure 4-15:	Peak stress deviation in percentage when an eccentric offset of 1 mm is present, plotted against varying delta.....	30
Figure 4-16:	The tensile stress deviation when the outer rollers are applying the load during eccentric loading. ....	31
Figure 4-17:	BMD & SFD comparison during an eccentric offset of 3 mm when the outer rollers are applying the load.....	31
Figure 4-18:	The peak stress error in percentage during an increasing eccentric offset for the two different loading cases. ....	31
Figure 4-19:	BMD comparison of the two eccentric load cases when the offset is 3 mm. ....	32
Figure 4-20:	Tensile stress deviation across the test surface during an increasing eccentric offset within real limits.....	32
Figure 4-21:	The tensile stress deviation when the outer rollers are applying the load during eccentric loading, within real limits.....	33
Figure 4-22:	Peak stress error when the inner rollers are rotated.....	34
Figure 4-23:	The normal stress surface profile of the specimen when the inner rollers are rotated 5 degrees.....	34
Figure 4-24:	Top view of the upper part of the 4PB test rig, rotated to show how the maximum rotation was calculated. The dotted outline is the ideal, or starting, position of the carrier.....	34

## List of Tables

Table 2-1:	The measured strain results in $\mu\text{m}/\text{m}$ for 7 different loading cases, the inherit error of the gauges are given by the 0kN loading case. ....	10
Table 3-1:	Dimension specification for the comparative specimen. ....	13
Table 3-2:	Table describing the boundary conditions for the recreated model. ....	13
Table 3-3:	Table describing the boundary conditions for the final model of the current specimen. ....	16
Table 3-4:	Table describing the essential limits for the GKN 4PB setup. ....	18
Table 5-1:	Optimal relations for the dimensions of 4PB specimen to lower peak stresses. ....	37



## List of acronyms and abbreviations

3PB	Three-Point Bending
4PB	Four-Point Bending
AM	Additive Manufacturing
BMD	Bending Moment Diagram
EQN	Equation
FEA	Finite Element Analysis
HCF	High Cycle Fatigue
LCF	Low Cycle Fatigue
RBM	Rigid Body Motion
SFD	Shear Force Diagram



# 1 Introduction

This chapter describes the specific problem that this thesis addresses, the context of the problem, the goals of this thesis project, and outlines the structure of the thesis.

## 1.1 Background

Producing components through AM is becoming more common within the aerospace industry [1], one company that is already using and planning to expand production through this method is GKN Aerospace [2]. This method makes it possible to create components with complex geometries, as well as making it possible to fuse multiple components into one. Furthermore, this type of manufacturing leads to less material waste. The main drawback with using AM is the surface roughness, which is an inherent loss of quality when manufacturing components through AM. This roughness is inevitable, and post processing is therefore required. This is crucial in areas where fatigue is of the utmost importance, since the surface roughness contributes to a shorter lifespan [3].

Mechanical testing is required to determine fatigue life properties of components, and a common method to test specifically surfaces is bend testing. This method makes it possible to investigate how surface conditions impact fatigue life which makes it a suitable method to evaluate AM surfaces. These tests are performed by applying a force in a way which produces a bending moment and consequently tensile stress on the surface. Two common setups for bend testing are three-point bending (3PB) and four-point bending (4PB). The main difference – as the name implies – is the number of contacts, or points, involved in the process. The result of using four points rather than three is a constant bending moment between the inner lines of contact, which means that it is possible to look at the entire surface between the inner rollers rather than a line directly beneath one inner roller. 4PB can therefore be used to evaluate larger surfaces. This makes it a desirable solution for GKN Aerospace since they are investigating AM surfaces with the goal of initiating cracks on the surface. A comparative diagram of these methods can be seen in Figure 1-1.

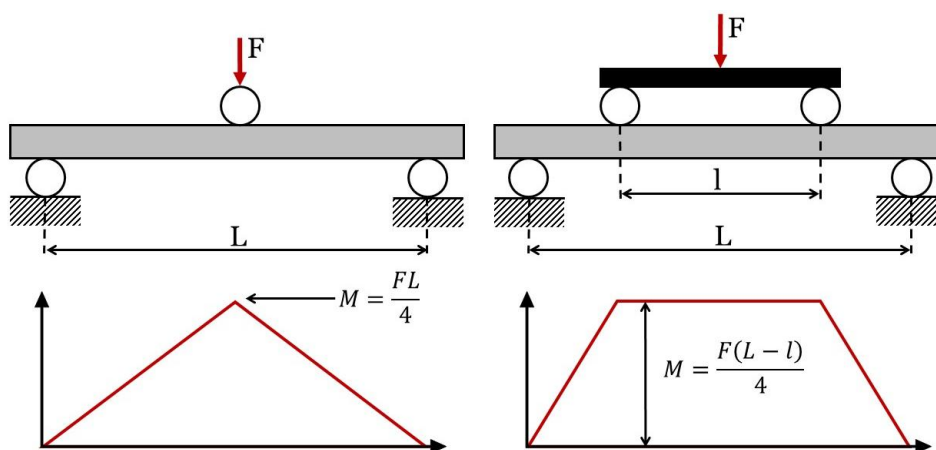


Figure 1-1: Diagram comparing 3PB (left) and 4PB (right), with their corresponding BMD.

It is essential that these testing methods provide consistent and valid results. The 4PB method provides an excellent solution for determining the fatigue performance of AM surfaces. This method therefore needs to be examined properly to establish the reliability and validity of this method.

## 1.2 Problem

The aim of this thesis was to examine and evaluate important aspects regarding 4PB, specifically focusing on aspects connected to the testing done at GKN Aerospace. A scientific article was recently brought to light at the mechanical testing department at GKN. The article, titled: *A self-aligning four-point bend testing rig and sample geometry effect in four-point bend fatigue* [4], presents findings regarding an error phenomenon known as wedging.

Wedging is an inherent error of 4PB which leads to localized stress peaks on the test surface, located shortly after the inner roller contact lines. These peaks are due to resulting disturbances from the compressive stresses of these inner rollers. In [4] the results show a stress increase of more than 5% above the nominal stress. Stress peaks of this magnitude would compromise the validity of fatigue tests performed where this phenomenon is present. Wedging is related to the geometry of the specimen and on the inner and outer rollers placement on the specimen and relation to each other.

There are other error sources that can introduce uncertainties. Eccentric loading, for example, which is the name for when the inner rollers are not centered to the outer rollers, or non-perpendicular loading: rotating the upper and/or lower part of the test rig making the contact line of the rollers non perpendicular to the specimen surface. 4PB testing is not yet fully understood when looking at how errors affect the results, which raises the question:

How do error sources affect four-point bending and can these errors be minimized by varying specimen geometry and roller placement?

## 1.3 Purpose

The purpose of this thesis project was to understand how the validity of 4PB testing can be influenced by errors, what these errors are and how they can be avoided or minimized. Further increasing the overall understanding of how 4PB works and how to implement this method properly in the aerospace industry.

Since 4PB fatigue testing is not yet standardized, testing is performed differently at different companies. Some use clamps fixturing of specimen, as well as multiple different specimen geometries, since these are yet to be specified. The result of not having a standardized testing method results in a lot of uncertainties, which could be catastrophic in the aerospace setting. The results of this thesis can help by implementing these findings to an international standard.

## 1.4 Goals

The goal of this thesis was to evaluate how the dimension and geometry of the specimen and the placement of the rollers affect the validity of 4PB testing. Furthermore, this was evaluated, and limits were decided to keep results within a total acceptable error margin of  $\pm 5\%$ .

The goal was divided into 4 questions:

1. To what extent do the specimen dimensions and geometry affect the occurrence and severity of local stress concentrations?
2. Can the position of the inner and outer rollers be optimized in a way which minimizes the occurrence of wedging without invalidating the test?
3. To what extent does the result get influenced by eccentric and non-perpendicular loading?
4. Which factors contribute the most to uncertainty during load when performing 4PB testing?

The thesis project was expected to generate geometry limits which help guide specimen design to minimize errors when 4PB testing is performed. It was also expected to generate suggested roller placement for the same reason. This will most likely decrease the uncertainties for this testing method and increase the overall understanding of 4PB.

## **1.5 Research Methodology**

The main problem arose from the findings of the Oxford article [4], and it was therefore decided to start the project by reviewing this article. An attempt to replicate the FEA results presented in [4] was made by building a simulation model in Ansys Workbench. The finished model was then used to investigate and find optimal specimen geometry and set limits to minimize errors, through simulations and parameter studies. Throughout the project, the model was discussed in-house as well as with independent researchers. The model was verified and validated by calculations, simulations and comparisons to measurements collected by calibrations performed at GKN Aerospace.

## **1.6 Delimitations**

The testing rig at GKN Aerospace was not evaluated since this introduces complexity to the simulations outside of this thesis scope. This means that factors like the height between the rollers and contact point in the machine and the spring forces used to keep the rollers in position were not taken into consideration.

Deformation of the roller was also neglected due to complexity outside of the scope. Furthermore, the friction forces that are present between the rollers and their contact lines on the specimen were neglected.

The error sources which this thesis focused on are wedging, eccentric loading and non-perpendicular loading. There are other error sources which are present in 4PB [5], but due to the time limit, the mentioned sources are the only ones which were investigated.

## **1.7 Structure of the Thesis**

Chapter 2 presents the relevant background information regarding 4PB and wedging, as well as the literature review and related work. Chapter 3 describes the entire process of the project, the methodology and how it was practically implemented. Chapter 4 presents the results and the analysis of these results, as well as the discussion. Chapter 5 presents the conclusions of this thesis project and recommended future work.



## 2 Background

In this chapter, the literature review and related works will be presented to provide relevant background information regarding the error sources, specimen geometry and mechanical testing. Additionally, the measurements used to validate the model are presented here.

### 2.1 Literature review

The Oxford article regarding 4PB test rigs and specimen design [4] is one of the major reasons this project has been performed. The purpose of the article and this project are one and the same: to understand and standardize the process of 4PB testing. The main goal was to evaluate their test rig and find an optimal relation between the loading/supporting roller span and the specimen height. These are investigated by FEA in Ansys followed up by testing a small batch of specimen with a specified setup. The nomenclature of this article was changed to correspond with this thesis project. A diagram from [4] with changed nomenclature can be seen below in Figure 2-1.

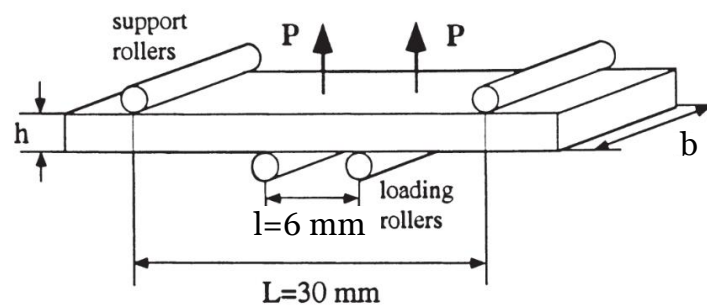


Figure 2-1: 4PB diagram from [4] with the same nomenclature as this thesis.

#### 2.1.1 Oxford article results

The results of this article are presented as graphs where the surface stress is plotted against the normalized position,  $x/l$ , between the inner rollers. What type of surface stress is not specified – e.g. if it is a normalized stress in the x-direction, equivalent von Mises, principal stress etc. – it is simply referred to as maximum stress. These graphs can be seen in Figure 2-2.

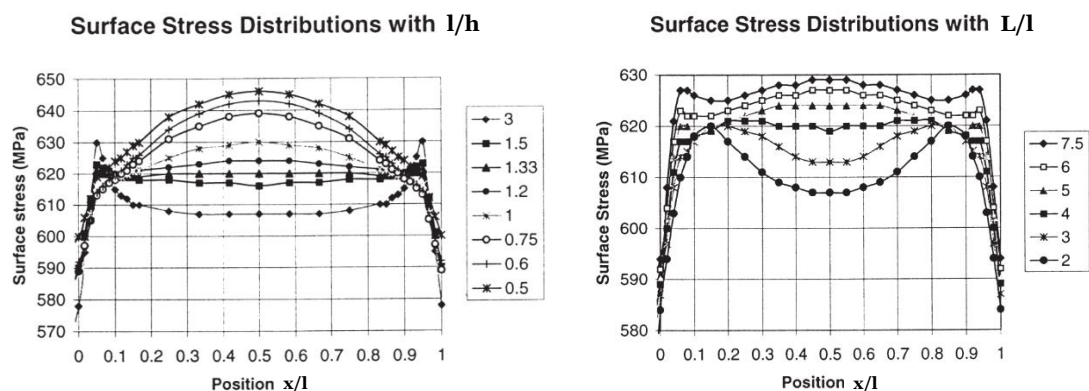


Figure 2-2: FEA results where the maximum stress is plotted against  $x/l$ , the normalized inner roller distance. The geometry is varied according to the  $l/h$  ratio (left) and  $L/l$  ratio (right).

In order to have a viable comparison between the different dimensions, all variations are simulated for a nominal stress of 600 MPa, which is calculated through eqn. (2-1) which is presented in [4].

$$\sigma_{nom} = \frac{3P(L-l)}{bh^2} \quad (2-1)$$

The load,  $P$ , is calculated by breaking it out of this equation, which is possible since the nominal stress,  $\sigma_{nom}$ , is defined as 600 MPa and the other dimensions –  $L$ ,  $l$ ,  $b$  &  $h$  – are known. The dimensions are varied in ratios, as seen in the legends in Figure 2-2:  $l/h$  and  $L/l$ . The maximum surface stress is then compared to nominal stress to find the peak stress error due to wedging. This error is seen to be as high as 7,5% when  $l/h = 0,5$  – which is a specimen with the dimensions:  $L \times l \times h \times b = 30 \times 6 \times 12 \times 1 \text{ mm}$ . A common theme among the specimen variations is that these never end up with a stress of 600 MPa. Which is deviant from the Euler-Bernoulli stress, defined in eqn. (2-1). The result closest to nominal stress ended up at approximately 608 MPa.

Wedging presents itself in the shape of localized stress peaks at the ends of the graphs in these results. The peaks appear close to the inner rollers – loading rollers in Figure 2-1 – contact with the opposite surface. These wedging stresses are due to the load being applied only on the surface. This creates concentrated compression stresses where the inner rollers contact the specimen which in turn disrupts the surface stress on the opposite surface [6]. This results in normal stress with a behavior seen in Figure 2-3 below.

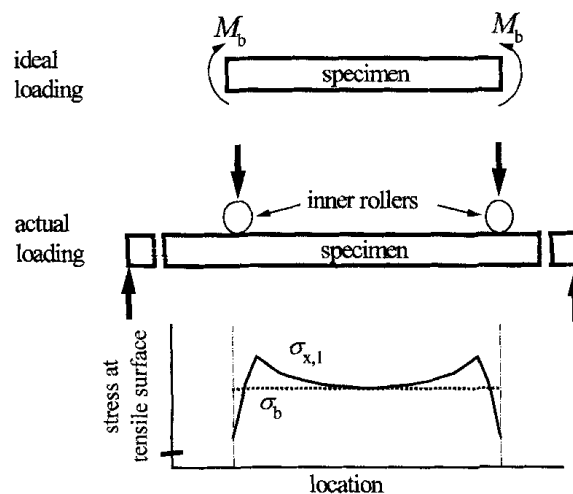


Figure 2-3: Surface stress during 4PB testing influenced by wedging. The dotted line is the calculated stress in ideal loading [7].

It is also important to note that some of the specimen variations do not experience this phenomenon. Instead, these have a single localized maxima at the middle of the test surface.

Based on these results, it is recommended to use 4PB specimen with the following ratios:  $l/h = 1,33$  and  $L/t = 5$  to avoid wedging stresses. These do still end up being approximately 3-4% larger than the nominal stress of 600 MPa.

### 2.1.2 Oxford simulation model

A schematic of the FEA model can be seen in Figure 2-4 below. The model consists of two regions: I and II. The difference being element size, both regions have an element size of  $h/20$  in the  $h$ -direction, but the regions differ in the  $l$ -direction: region I has a size of  $(L - l)/50$  and region II has a size of  $l/30$ . Ending up with a total of 800 surface elements. The simulation is performed in 2D, with a theoretical width of 1 mm. The boundary conditions are composed of a line load at the indicated “Load P” arrow, a symmetry plane at the middle point of the specimen – indicated by two rows of dots linked together – and an unspecified support at the opposite end.

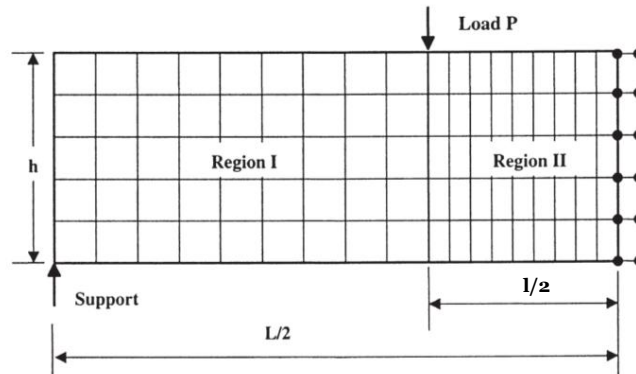


Figure 2-4: Schematic of FEA model used by [4] with new nomenclature.

This model is vague; there is some important information missing. For example, the unspecified support, which was assumed to be a displacement support locked from moving vertically. The load is not specified further than being a line contact and calculated from eqn. (2-1). Furthermore, it is not specified if the elements are linear or of the second order. The type of stress is, as mentioned earlier, not specified further than: *maximum bending stress on the surface*. The surface is assumed to be the lower line of region II, and the type of stress was assumed as directional stress along this line.

### 2.1.3 Oxford article summary

The results from this article raise a few questions, one of these was an important aspect of this project: how severe are these wedging stresses and how can they be avoided? Furthermore, the results seem off. Firstly, none of these coincide with beam theory equations; nominal stress is never achieved. The recommended solutions exceed it by 3-4%, which is significant when compared to a total allowed error of 5% which would significantly impact fatigue-life properties. The recommended ratio of  $L/l = 5$  leads to a very long specimen compared to the length of the testing surface. A specimen with a length of 100 mm would have a testing surface length of 20 mm, which might not be ideal when a larger test surface is needed with a limited space in the testing rig. Combined with the recommended  $l/h$  ratio, the thickness of the specimen would need to be approximately 15 mm.

This raises awareness of issues that might otherwise go unnoticed, but the results do not add up. The simulated FEA results do not match calculated results from eqn. (2-1) which lead to the conclusion that beam theory is invalid for these cases according to [4]. It is simply acknowledged and accepted that 4PB results with stresses approximately 3-4% larger than nominal stress.

### 2.1.4 Alternate geometry

Alternative geometries have also been used in 4PB testing. One of these can be seen below in Figure 2-5. This geometry resembles a dog bone type specimen which has been cut in half along its length. This geometry has been used to inspect how the build angle impacts fatigue life of AM specimen [8].

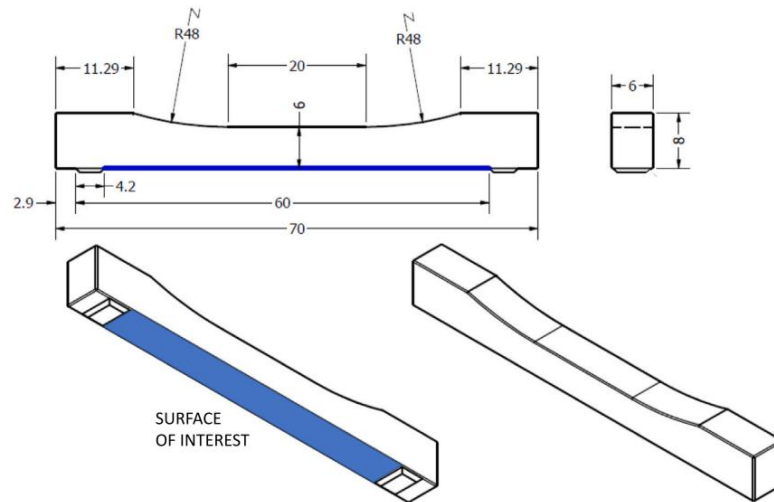


Figure 2-5: The specimen used by [8] implemented into 4PB fatigue tests of AM surfaces.

## 2.2 Mechanical Testing

Mechanical testing can be performed using different methods, such as bend testing, and is an important aspect of ensuring the safety of the final product. The goal of mechanical testing is to evaluate material properties of components. Hardness, tensile strength and fatigue life are examples of what can be determined through tests like Rockwell, tensile and LCF respectively. Furthermore, mechanical testing follows strict guidelines defined in international standards. This is to ensure that results from these tests can be compared even if two separate entities perform two separate tests with the same method. Without these guidelines there are no guaranties that tests can be compared, which introduces uncertainties. How these tests are performed differs and depends on the international standards [9].

### 2.2.1 Flexural testing

The mechanical testing setup which has been evaluated in this thesis project, 4PB, falls under the category of flexural – or bend – testing. The two most common types of flexural tests are three-point bending and four-point bending. Bend testing is commonly used for composites and polymers, and other flexible materials and these are used to assess material properties like flexural strength and fatigue life [10]. It is also suitable for AM surfaces due to the stress being mainly on the surface and theoretically equal along the test surface.

The functions of these tests are the same: a sample specimen is placed in a fixture and experiences a bending moment in some way. The difference being how many points/lines of contact are present in the testing procedure, see Figure 1-1. Furthermore, 3PB evaluates a line while 4PB evaluates a surface, making 4PB more suitable for evaluating AM surfaces.

### 2.2.2 Mechanical testing at GKN

A variety of mechanical tests are performed at GKN Aerospace. Most of these tests follow international standards, except for 4PB. The reasoning behind using 4PB – even though it is not standardized – is due to its capability of evaluating surfaces. Specifically, how the inherent roughness of AM surfaces impacts fatigue life properties. Since this bend testing method has a theoretically uniform tensile stress along the entire test surface, it is the ideal method for initiating cracks on the surface.

Furthermore, this leads to the reason for the thesis project: evaluating and providing resources to increase awareness and help with the standardization of this test method. The current way the test is set up can be seen in Appendix A. One common specimen used in 4PB is a rectangular block, a drawing of which can be seen in Appendix B. Fatigue testing has been performed on AM specimens with surfaces which were either as built or post processed. These have been compared to each other to determine how as-built surfaces affect fatigue life properties. The results of these tests can be assumed to be valid enough to gain some understanding regarding the surface influence on fatigue life; because the only difference in these tests is the surface condition of the specimen, and both types are performed in the same machine.

However, errors like wedging causes uncertainties that are obstructing the results from being completely validated. Wedging causes localized stresses on the test surface. These might be what is initiating cracks on the surface, rather than irregularities due to the AM surface roughness. It cannot be ruled out that the 4PB tests that are performed look at the entire surface or if the cracks are due to peak stress.

### 2.3 GKN 4PB Test Setup

The current testing rig at GKN Aerospace is described in an internal document [11]. The rig in question can be seen as a diagram in Appendix A. Moreover, a drawing of the specimen was acquired, and a simplified version of this with measurements in metric units can be seen in Appendix B.

There have been earlier versions of this testing setup, and in this document, the changes that were made from the last one are shown and discussed. To summarize: the constraints have been reworked to let the rollers move with the curvature of the specimen during loading (outer rollers are allowed to move outwards and vice versa), the distance between crosshead and actuator was reduced and the lower fixture was mounted directly on the hydraulic piston to increase the stability of the rig. Furthermore, the springs keeping the rollers in place were changed to O-rings, which increased the force keeping the rollers in place, and 3D-printed alignment spacers were introduced to achieve a better placement of the specimen and fixtures. Additionally, micro strain gauges were used to calibrate the test. The placement of these gauges can be seen in Figure 2-6.

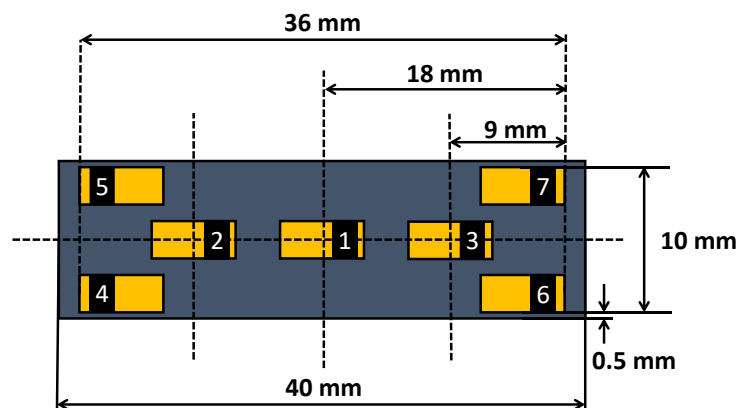


Figure 2-6: The micro strain gauge placements on the specimen test surface.

The results of these measurements were provided by the laboratory personnel that performed the calibration, and some of these measurements are presented below in Table 2-1.

**Table 2-1: The measured strain results in  $\mu\text{m}/\text{m}$  for 7 different loading cases, the inherit error of the gauges are given by the 0kN loading case.**

Load [kN]	Ch 1	Ch 2	Ch 3	Ch 4	Ch 5	Ch 6	Ch 7
0	39.414	39.107	38.778	39.409	38.371	39.247	38.014
0.1	101.022	100.148	99.813	102.900	99.934	99.735	99.577
1	682.750	679.358	677.848	691.643	687.141	680.124	681.967
2	1331.148	1321.472	1324.163	1343.552	1337.186	1330.787	1333.989
3	1976.079	1960.975	1967.275	1992.571	1984.412	1978.958	1983.068
4	2622.242	2602.064	2611.171	2643.483	2632.509	2628.250	2632.120
5	3267.171	3241.548	3254.044	3293.664	3280.057	3277.096	3280.570

It is also worth noting that the micro-strain deviation resulted in less than 2.5% for the new setup and specimen according to [11].

## 2.4 Summary

To summarize, the 4PB testing method has yet to be properly indoctrinated into a standardized procedure. It has been used as a flexure testing method for brittle materials for a long time. [7] refers to works going back to the late 1980s. The method is clearly being used in varying ways, and it is therefore hard to compare results produced by different parties. Furthermore, there are still a lot of uncertainties regarding 4PB which leads to further confusion and varying degrees of validity. A great example of this is the analysis performed in [4] where the results of the simulation deviate significantly from calculated and expected results. Additionally, there are no specifications regarding either specimen geometry or how the testing rig is composed.

Some of these concepts were used in this thesis project to evaluate the 4PB method: different geometries, simulations of errors – such as wedging and eccentric loading – and the strain measurements were used to validate the model.

### 3 Methodology & Implementation

This chapter will describe the engineering methods and how they were practically implemented to carry through with this thesis project.

#### 3.1 Beam Theory Calculations

Before building the model beam theory calculations took place. Regular beam splitting provided the formula for the bending moment as well as the shear forces throughout a common 4PB specimen seen in Appendix B. A graph showing the BMD and SFD for this specimen can be seen in Figure 3-1. The formula for the bending moment on the test surface between the inner rollers is seen below in equation (3-1) and the shear forces are  $F/2$  and  $-F/2$  for the distances between the inner and outer rollers on each side of the test surface.

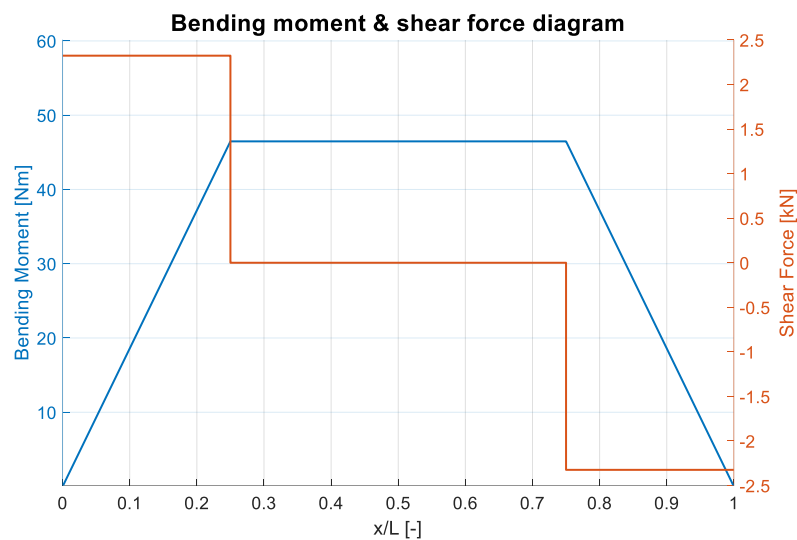


Figure 3-1: BMD and SFD for a common 4PB specimen, inner rollers are placed at the ends of the horizontal moment line and outer rollers are placed at the ends of the moment curve.

$$M = \frac{F}{4}(L - l) \quad (3-1)$$

Where  $F$  is the applied load,  $L$  is the distance between the outer rollers and  $l$  the distance between the inner rollers, the variables can be seen in the diagram of the specimen seen in Figure 3-2.

Additionally, the bending moment on the left side of the test surface is given by eqn. (3-2), and eqn. (3-3) shows the resulting bending moment on the right:

$$M = \frac{F}{2}x, \quad 0 \leq x \leq \frac{1}{2}(L - l) \quad (3-2)$$

$$M = \frac{F}{2}(x - l), \quad \frac{1}{2}(L + l) \leq x \leq L \quad (3-3)$$

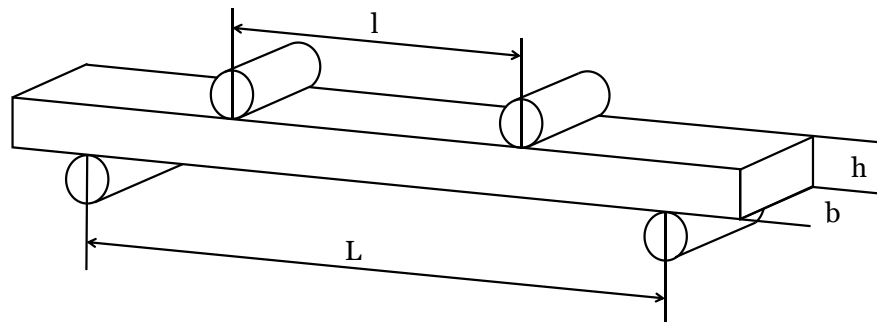


**Figure 3-2:** Diagram of a 4PB specimen with rollers to define the important dimensions.

The maximum tensile stress can be calculated by dividing the bending moment with the bending resistance,  $Wb$ , which in the case of a beam with a rectangular cross section equals the equation below.

The tensile stress calculation can therefore be written as follows:

$$\sigma = \frac{3F(L - l)}{2bh^2} \quad (3-5)$$

Additionally, this equation is equal to the equation provided by [4] (eqn. (2-1)). Consequently, the applied load can be extracted:

$$F = \frac{2bh^2}{3(L - l)} \quad (3-6)$$

Eqn. (3-6) was used to determine the magnitude of the applied force which kept the nominal stress at 600 MPa with varying geometries. This nominal stress value was primarily chosen to correlate to [4], but it is also a reasonable stress for the alloys being tested at GKN. It was therefore determined to continue with 600 MPa to remain consistent throughout the thesis project.

### 3.2 Building the Simulation Model

It was determined that if the FEA model built in this thesis project could replicate the results of [4], it could be easily verified – as well as allowing for a comparative model which would be the basis for the geometry study. This model is described in Chapter 2.1.2. and as discussed, the description is vague. Consequently, the recreation was performed by choosing one of the simulated specimen geometries presented in [4]. The dimensions of this chosen specimen are seen in Table 3-1.

**Table 3-1: Dimension specification for the comparative specimen.**

Location of dimension	Designation	Length [mm]
Distance between outer rollers	$L$	30.0
Distance between inner rollers	$l$	6.0
Specimen height	$h$	2.0
Specimen breadth (theoretical)	$b$	1.0

Due to the nature of the simulation being in 2D, the breadth of the specimen is theoretical. This specimen was chosen because it showed the most severe wedging occurrences, as well as being the closest result to the specified nominal stress of 600 MPa. The model was built in Ansys Workbench 2024 R2, specifically in a static structural subsystem. The reason for using Ansys is because this is the preferred FEA software at GKN Aerospace. The recreated comparison model is seen in Figure 3-3.

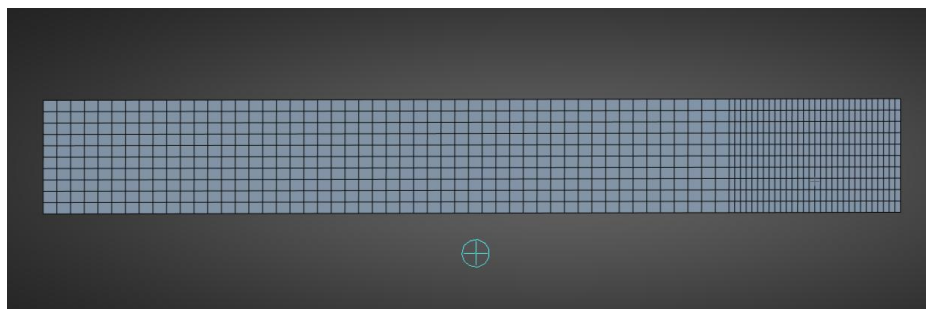


**Figure 3-3: The resulting mesh of the recreated 2D model.**

The mesh was built according to [4]: 800 quadrilateral surface elements with a region of smaller elements within the inner rollers. The boundary conditions are shown in Figure 3-4 and defined in Table 3-2 below. Additionally, stress on the test surface was defined as normal stress along the surface axis – pink line seen in Figure 3-4 – which gathered stress through element average.

**Table 3-2: Table describing the boundary conditions for the recreated model.**

Boundary condition	Label	Value/Type	Role
Displacement Support	<b>A</b>	Locked Vertically	<i>Outer Roller</i>
Displacement Support	<b>B</b>	Locked Horizontally	<i>Symmetry Plane</i>
Point Force	<b>C</b>	33.333 N	<i>Inner Roller</i>



**Figure 3-4: The boundary conditions of the model recreation, test surface is indicated via the pink line.**

The resulting primary comparison of the results for this specimen are seen below in Figure 3-5. The results differ significantly, and because of this, the model was scrutinized.

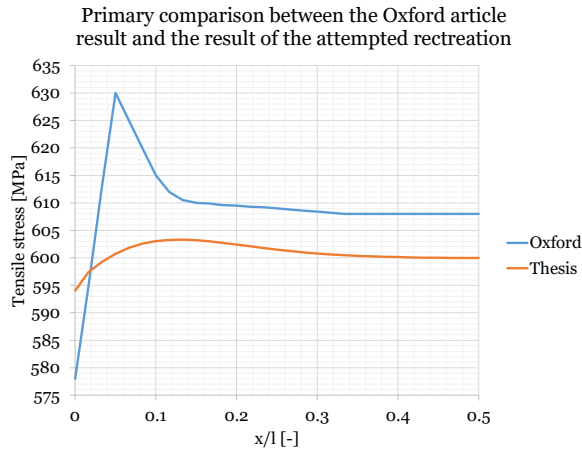


**Figure 3-5:** Primary comparison between [4] and the FEA model of this thesis.

Since the model description was vague to begin with, discrepancies were expected, although not to this degree. Firstly, the element order was changed to linear instead of quadratic. Secondly, the effect of using either plane stress or plane strain was compared. The results can be seen in Figure 3-6.

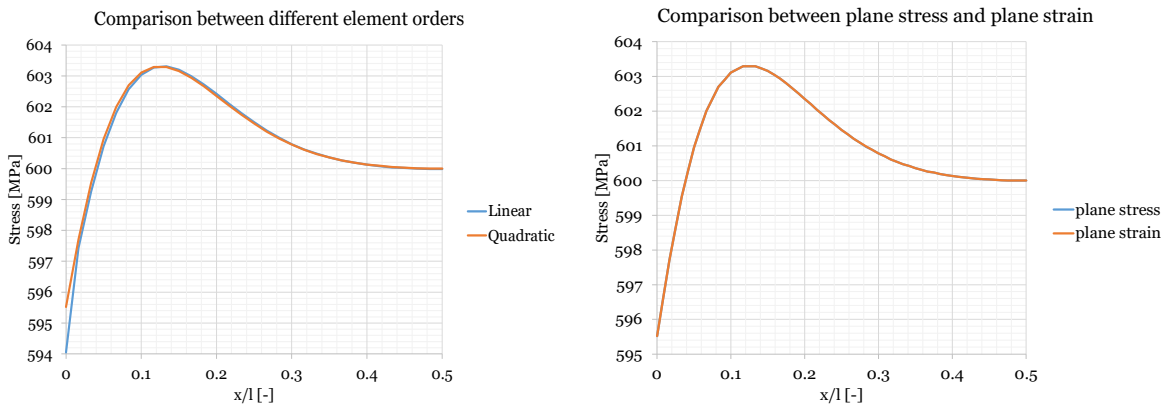


**Figure 3-6:** Element order comparison (left) and comparison between plane stress and plane strain (right).

Thirdly, the stress type was compared. These evaluated stress types were normal, principal and equivalent von Mises stress. Finally, the model was built in 3D to identify the effect of having an actual width and how it would impact the results. These comparisons can be seen in Figure 3-7.

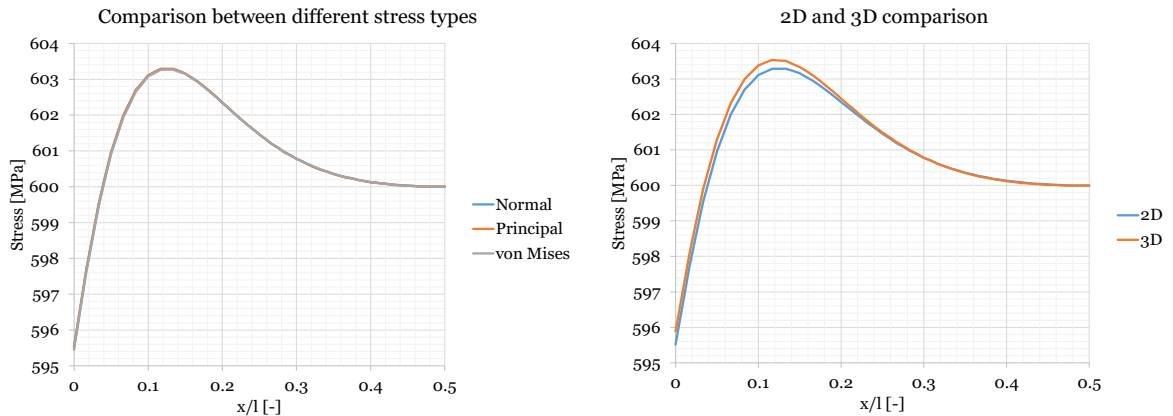


**Figure 3-7:** The stress behavior when scoping for different stress types (left) and comparing the behavior in 2D and 3D (right).

After this comparative study was performed, it was believed that the model produced more reliable results than those of [4]. The results were also presented and discussed with supervisors and solid mechanics researchers at University West. In addition to the miniscule differences seen when trying different model setups, the results matched those calculated through beam theory: the tensile stress ended up equal to the nominal stress around the middle of the test surface. The behavior also matches the proposed wedging description presented by [7].

### 3.3 Final Model

For the parameter study to work as intended, the model was created in Ansys Spaceclaim. In this built-in CAD software, the parameterization of each dimension was made possible since every action was based on the previous action. Meaning that these dimensions could relate to each other without overlapping, which was an occurring error when trying to implement parameters in Ansys Discovery. When the model was completed, some parameters were changed to calculations to streamline the study. The force, for example, implemented as a function dependent on the parameters containing the different lengths to keep the tensile stress equal to the nominal stress of 600 MPa – eqn. (3-6).

Furthermore, the model was constructed with 2<sup>nd</sup> order elements and scoping for normal stress. This model was determined, through discussions, to be reliable due to consistent results. Moving forward, the model was adjusted to reflect the common specimen and the current 4PB set-up at GKN Aerospace. It was implemented in 3D instead of 2D to better reflect on reality and to perform studies which required actual width. The dimensions of the final model were designed to be varied but the measurements of the baseline model were based on those of Appendix B. This model can be seen in Figure 3-8.

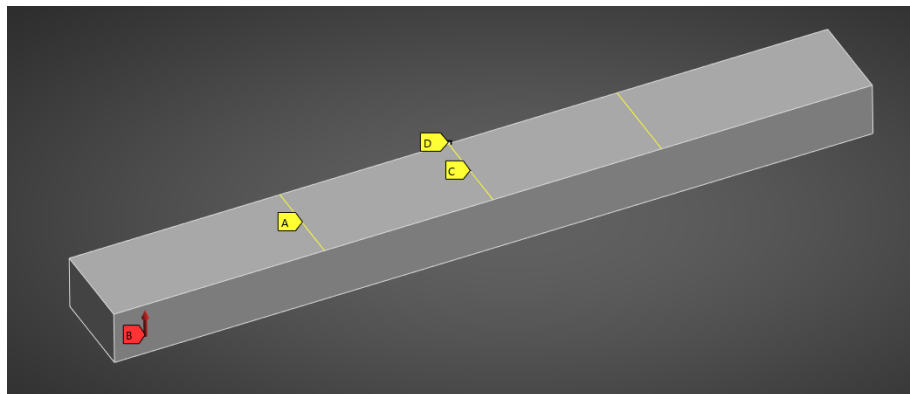


Figure 3-8: Top view of the baseline 3D model based on a common 4PB specimen.

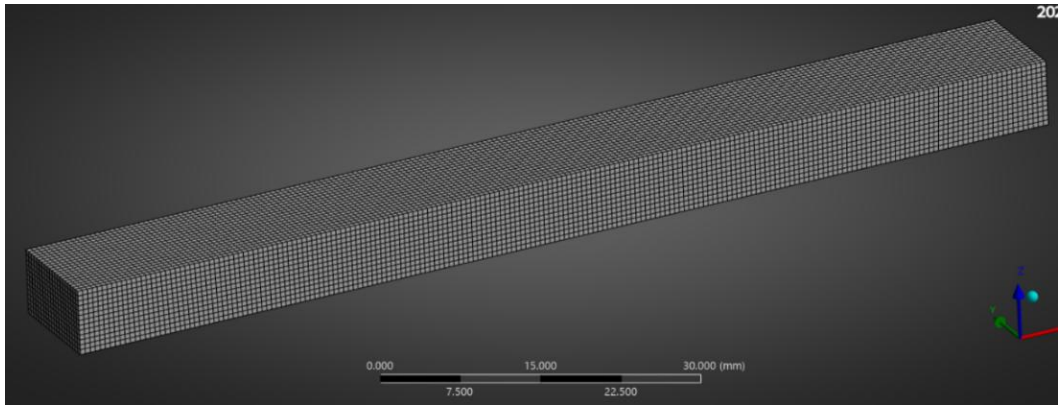
The boundary conditions are described in

Table 3-3. In addition to these boundary conditions, a small distance of 5 mm was added outside of each outer roller contact to avoid having the forces directly applied to the ends of the specimen. Because the model was implemented in 3D, rigid body motion needed to be prevented. This was accomplished by introducing two displacement supports: C and D. These were placed by implementing a line at the middle of the top surface of the specimen. This line was prevented from moving along the specimen – which it should not in an ideal scenario – and one of its vertices were set to prevent sideways motion (also an ideal condition). Another prevention of RBM was used to control if these applied supports were correct: weak springs. This adds 3 springs with small forces at each corner of the bounding box with the sole purpose of preventing RBM. These were only used when controlling that the actual supports were correct and not interfering with the result and not a part of the final simulations.

**Table 3-3:** Table describing the boundary conditions for the final model of the current specimen.

<b>Boundary condition</b>	<b>Label</b>	<b>Value/Type</b>	<b>Role</b>
Displacement Support	<b>A</b>	Locked Vertically	<i>Inner Rollers</i>
Line Force	<b>B</b>	4647.5 N	<i>Outer Rollers</i>
Displacement Support	<b>C</b>	Locked Horizontally	<i>Prevent Rigid Body Motion</i>
Displacement Support	<b>D</b>	Locked Sideways	<i>Prevent Rigid Body Motion</i>

The final mesh was made with cuboid elements of the 2<sup>nd</sup> order with a side of approximately 0.5 mm for the baseline specimen, which resulted in a total of 52 000 elements. This mesh can be seen in Figure 3-9. The elements were defined as divisions along edges and the number of elements remained constant throughout the project.



**Figure 3-9:** The mesh of the 3D model baseline specimen.

Since the number of elements remained constant, the element size was varied during the later performed parameter studies. A mesh refinement study was therefore performed to investigate the effect the number of elements had on the results. This comparison was made on a specimen with the same dimensions as the baseline except for the distance between the inner rollers, *l*, which was set to 60 mm to achieve a larger test surface. The results of this can be viewed below in Figure 3-10.

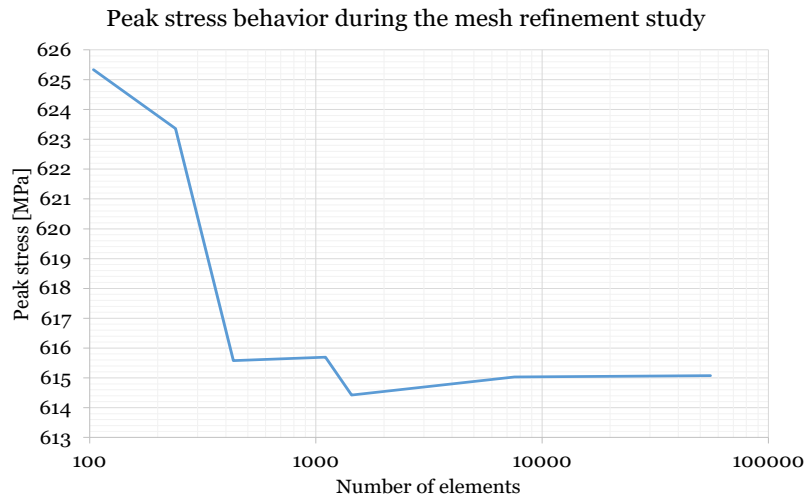


**Figure 3-10:** Resulting peak stress behavior when the number of elements, and consequently size, varies.

When the greatest number of elements are used in the refinement study, the peak stress caused by wedging for this geometry ends up at 615 MPa. When there are more than 400 elements in the model the deviation from this peak stress is at most  $\pm 0.08\%$ . Continuing with the model, the result scoping was created by implementing a path along the middle of the test surface (see Figure 3-11) which captures the normal stress along this axis, the stress values are gathered from element average.

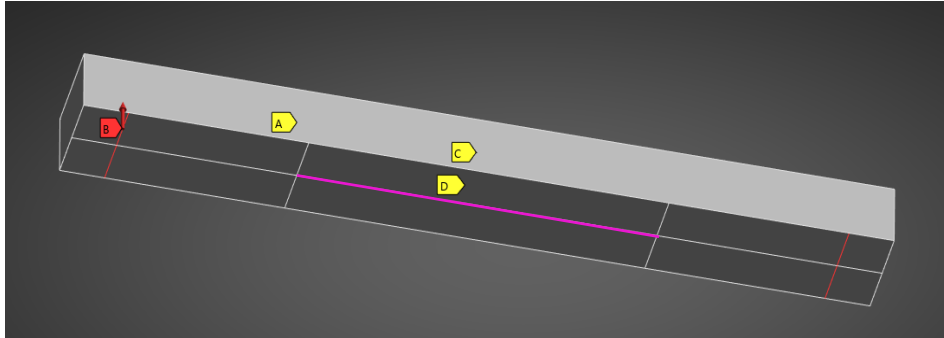


Figure 3-11: Bottom view of the 3D model baseline specimen. The red lines are outer roller contacts, and the pink line is where the stress data is collected.

### 3.4 Model Validation

The model was validated by comparing the model results to real measurements. The measurements were collected as a part of calibrating the new test setup at GKN Aerospace [11]. The collected data is seen in Table 2-1. The model was updated to match the specimen used in the calibration and scoping paths were implemented where the micro strain gauges were placed. The micro strain gauge placements are seen in Figure 2-6 and the scoping paths are seen in Figure 3-12. The resulting comparison can be seen in Chapter 4.2.

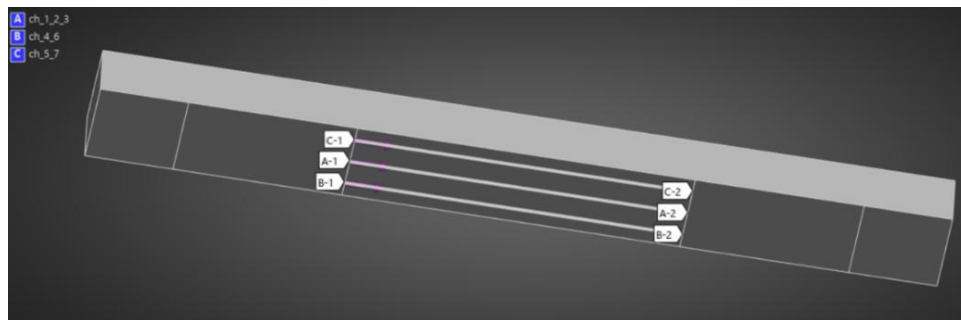


Figure 3-12: Model used for strain verification with the 3 paths marked out and named after the involved channels.

### 3.5 Parameter Study

Consequently, there were a lot of different parameters that could be varied to find the optimal geometry and, to structure the following parameter studies it was decided to investigate ratios and relations between these parameters. The first part of the study was to evaluate the proposed ideal ratios from [4]. Secondly, the alternate geometry [8] was investigated. Thirdly, the cross section, or height-breadth relation, was evaluated and finally the inner-outer roller relation was investigated. The parameters were limited by the 4PB testing setup at GKN, which are defined in Table 3-4. The limits were implemented in the parameter study.

**Table 3-4:** Table describing the essential limits for the GKN 4PB setup.

Variable	Max	Min	Unit
$L$	220.0	20.0	mm
$l$	120.0	15.0	mm
$F$	1.5	10.0	kN

### 3.5.1 Proposed ideal ratios

The ideal ratios that were proposed by [4] can be seen in Chapter 2.1.1. There are real cases where these ratios are being used for 4PB testing, one such specimen is being used at Linköping University [12]. The distance between the rollers is limited to only 12 mm, and already this is something which is not suitable for GKN Aerospace, since a large test surface is needed for the AM surface fatigue testing. Furthermore, this specimen had a resulting surface stress behavior more similar to 3PB than 4PB, with a surface of equal stress approximately 3 mm long. This behavior was therefore named pseudo-3PB, and the resulting stress peak ended up being 2.25% larger than nominal stress. The stress curve can be seen below in Figure 3-13.

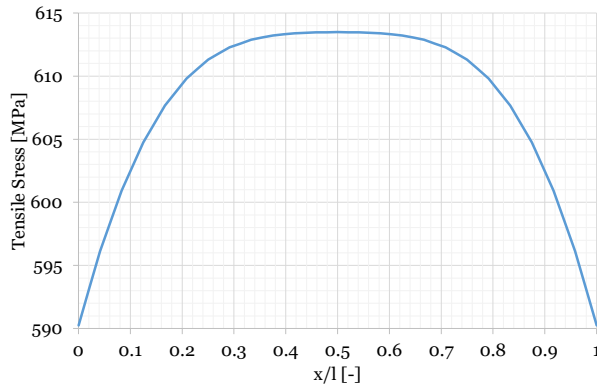


**Figure 3-13:** The normal stress along the test surface for a specimen with dimensions seen in [12] which is based on the ratios stated in [4]. Nominal stress is 600 MPa.

With these dimensions as a base, the pseudo-3PB behavior was investigated by varying the specimen thickness, inner roller distance and outer roller distance. The results can be seen in Appendix C. The takeaway from this study was that the proposed ratios produce the crossover point from 4PB to pseudo-3PB. Increasing specimen thickness leads to a larger stress deviation and decreasing the inner roller distance moves the behavior closer to 3PB, as expected. Additionally, increasing the distance between the outer rollers lowers stress deviation.

### 3.5.2 Alternate geometry evaluation

The parameter study continued by investigating different geometries. The geometry chosen to be investigated was the alternate geometry described in Chapter 2.1.4, where its shape and dimensions are described in Figure 2-5. Specimens of this geometry are also being used for 4PB testing [8]. This was compared to a specimen of the same length and roller placement:  $L_{tot} = 70 \text{ mm}$ ,  $L = 60 \text{ mm}$  and  $l = 20 \text{ mm}$ , but without the radii. This rectangular specimen had a cross section of  $6 \times 6 \text{ mm}^2$  instead. The result of this comparison is seen in Figure 4-3.

For the rest of the parameter and error studies the baseline specimen was chosen to be the common specimen geometry, dimensions of which are seen in Appendix B.

### 3.5.3 Cross section study

The next phase of the procedure was to investigate how the breadth and height of the specimen influenced the wedging error. The height,  $h$ , varied from 2 to 8 mm with steps of 1 mm and the breadth,  $b$ , varied from 4 to 16 mm in steps of 2 mm. The results are seen in Figure 4-4.

### 3.5.4 Roller placement study

The final part of the parameter study was to investigate the relationship between the rollers to find an optimal placement. The horizontal distance from one outer roller to the nearest inner roller was given a parameter,  $\delta$ . Its implementation is seen in Figure 3-14.

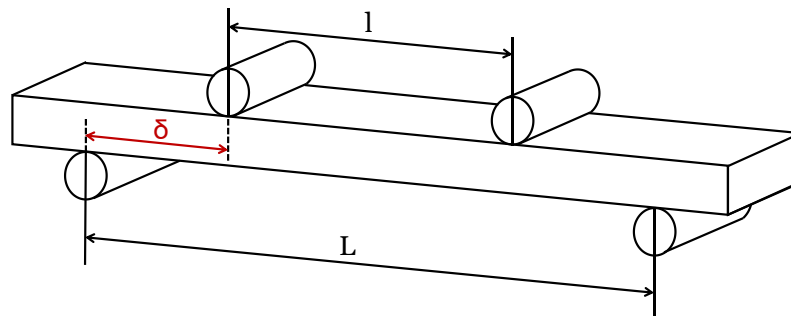


Figure 3-14: Diagram of how the parameter  $\delta$  is defined.

$\delta$  and  $L$  varied accordingly:  $\delta$  varied from 5 to 35 mm in steps of 5 mm and  $L$  varied from 80 to 140 mm in steps of 10 mm. The results of this study can be seen in Figure 4-9.

## 3.6 Error Sensitivity Study

This study investigates how sensitive 4PB is to eccentric and non-perpendicular loading conditions and was performed to find tolerances to keep the total error within  $\pm 5\%$

### 3.6.1 Eccentric loading

Firstly, a study on how eccentric loading influences error was performed. Eccentric loading implies that one pair of rollers is not centered with the other pair. To replicate this a variable,  $\alpha$ , is introduced and works as an eccentric offset for the inner rollers – moving them towards one direction while keeping the outer rollers stationary and centered with the specimen. A diagram describing this scenario is seen in Figure 3-15.

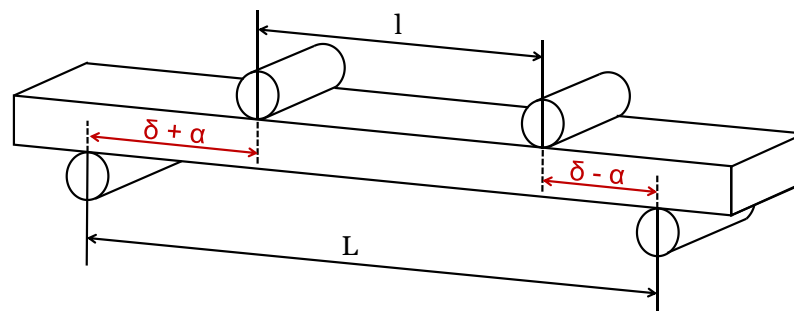


Figure 3-15: Eccentric loading diagram where  $\alpha$  is the eccentric offset parameter.

In an ideal case, where everything is symmetrical, the load of each individual roller is equal to  $F/2$ . When asymmetry is introduced – as described in the diagram above (Figure 3-15) – the configuration of the 4PB test set-up matters. In the case of GKN Aerospace, the rig is arranged in a way which ensures that the inner rollers are always applying a load of  $F/2$  each onto the specimen, even if the outer rollers are applying the actual load. The outer rollers, on the other hand, apply a force which is dependent on the introduced variable  $\alpha$ . This was implemented in the model and investigated. The opposite case was also studied, and the results differed significantly.

The reaction forces which depended on  $\alpha$  were calculated through beam splitting, the reaction forces also depended on which rollers they were applied through. A diagram which shows the case at GKN – where the inner rollers are applying an equal load – can be seen below in Figure 3-16.

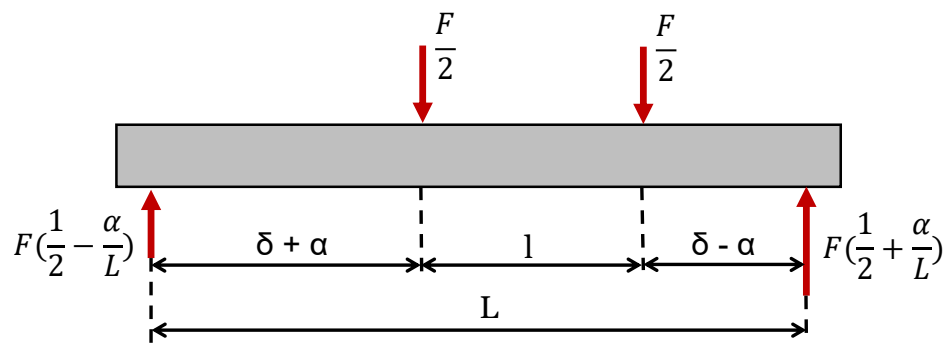


Figure 3-16: Eccentric load diagram, when inner rollers are applying the load.

The opposite case, where the inner rollers are applying unequal reaction forces instead, is seen in the diagram in Figure 3-17.

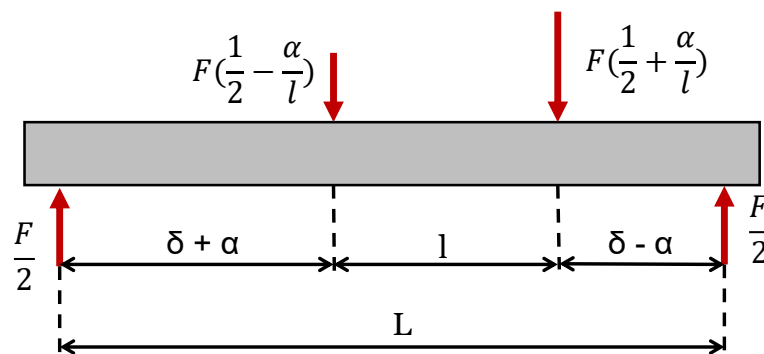


Figure 3-17: Eccentric load diagram, when outer rollers are applying the load.

The reaction forces are reliant on the eccentric offset and the distance between the supporting rollers, and this ratio becomes vastly different since the inner roller distance is shorter than the outer roller distance. This indicates that the peak stress due to eccentric load increases more rapidly in cases where the inner rollers are not applying an equal load. The severity of this offset was discussed with the laboratory personnel. The simulated case of moving the inner rollers relative to the outer rollers is an intuitively realistic take on the issue: according to the laboratory personnel, the outer rollers are assumed to be completely stationary due to the way they are implemented in the 4PB setup at GKN. The inner rollers, on the other hand, are assumed to have some movement.

This movement is limited by spacers and guides which prevent the rollers from moving more than  $\pm 0.2$  mm from the centerline. As a precaution, the limit was increased to  $\pm 0.5$  mm and results within this limit are seen in Figure 4-20 and Figure 4-21.

### 3.6.2 Non-perpendicular loading

Secondly, it was decided to study the effect of non-perpendicular loading. This was implemented by adding an angle parameter which rotated the inner and outer rollers lines of contact in the simulation model. The lines were kept parallel to simulate the entire upper part of the 4PB setup to rotate along its centerline. This process was repeated for the outer rollers on the lower part of the rig.

A representative diagram of this parameter can be seen below in Figure 3-18 for inner roller rotation and Figure 3-19 for outer roller rotation.

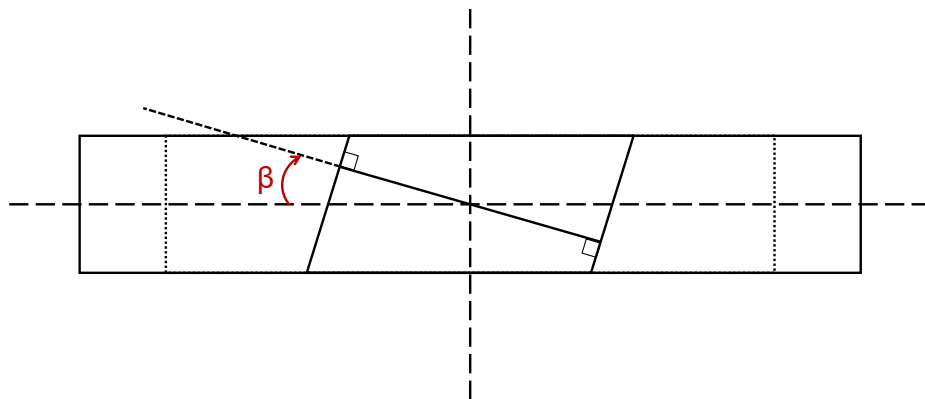


Figure 3-18: Diagram of how the inner rollers lines of contact were rotated with a rotational parameter,  $\beta$ .

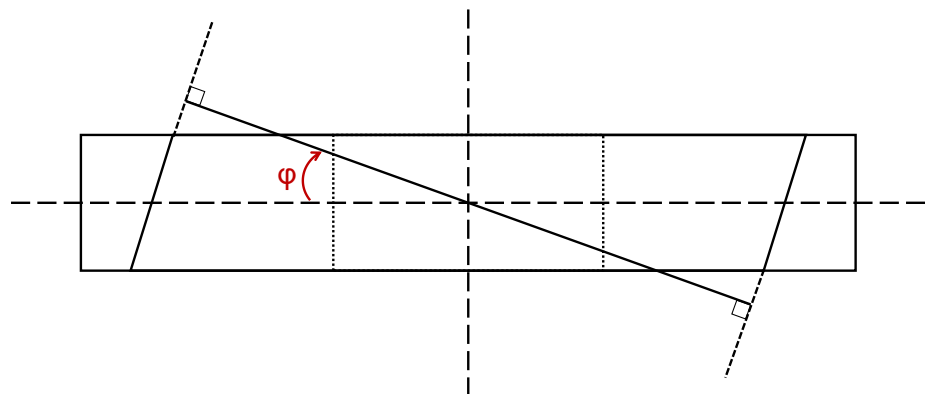


Figure 3-19: Diagram of how the outer rollers lines of contact were rotated with a rotational parameter,  $\phi$ .

After further discussion with the laboratory personnel, it was confirmed that the inner rollers had some movement capabilities in this manner as well. An interesting discovery when performing this study was that only rotation of the inner rollers resulted in a change in peak stress. Both sets of rollers were rotated a total of 5 degrees in different combinations. The results and analysis of these results are presented in Chapter 4.4.2.



## 4 Results and Analysis

The results of this thesis project will be presented, analyzed and discussed in this chapter. They are categorized according to Chapter 3: firstly, the results related to the FEA model and its validation are presented. Secondly, the parameter study results, and finally the error sensitivity study results.

### 4.1 FEA Model Comparison

The ultimate comparison of the results from this thesis project simulation and [4] can be seen in Figure 4-1 with the specimen dimensions described in Table 3-1.

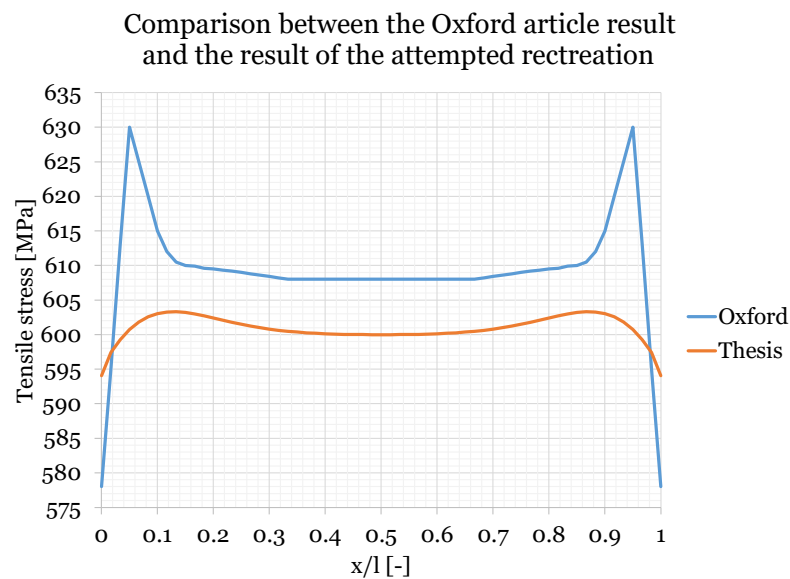


**Figure 4-1:** Comparison between the attempted recreation and the results presented in [4], for a specimen with  $l/h = 3$ .

As described in chapter 3.2, multiple different simulations were performed to achieve similar results, however the results were not possible to replicate. Continuing, the results of the article do not match the calculated results through Euler Bernoulli beam theory calculations (Chapter 3.1). Additionally, the results of [4] do not match the theoretical results presented in [7]. In contrast, the simulations performed in this thesis project match the expected behavior described in [7], the Euler Bernoulli beam theory and real measurements.

### 4.2 Model Validity Analysis

The validity of this simulation model has been evaluated through comparison with measured strain provided by a calibration performed at GKN Aerospace, these measurements can be seen in Table 2-1. The comparison between the measured and simulated strain can be seen in Figure 4-2. The decision was to compare measured strain from the 5 kN case with simulated strain for the same load. The reason for using 5 kN was due to the load being circa 4.7 kN to achieve a nominal stress of 600 MPa for the baseline specimen, which was also the specimen used in the calibration.

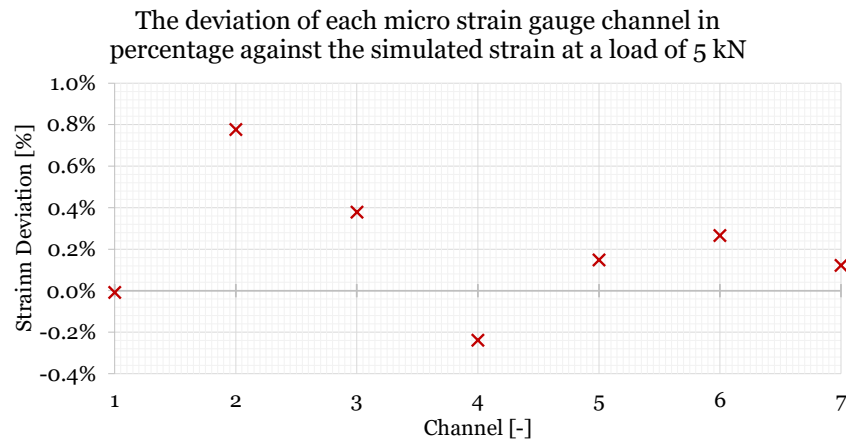


**Figure 4-2:** Strain deviation of the measured strain compared to the simulated strain at a load of 5 kN.

The location of each channel can be seen in Figure 2-6. The largest deviation is seen on channel 2, which is approximately 0.8%. Since all channels are within  $\pm 1\%$  the model represents the real 4PB test to a satisfactory degree. Furthermore, channels 4, 5, 6 and 7 are shown to have a slightly larger strain than channel 1, 2 and 3 – which can be seen in Table 2-1 where the load is 5 kN. Which is due to their placement lining up with the inner slopes of the occurring wedging stresses.

### 4.3 Parameter Study Results

The results of the parameter studies are presented here.

#### 4.3.1 Alternate geometry comparison

After evaluating at the proposed ideal specimen as described in Chapter 3.5.1 – where these proved to lead to a pseudo-3PB behavior – a comparison between the alternate geometry [8] and a rectangular block with the same cross section, length and roller placement was performed. The result of this comparison is seen in Figure 4-3.

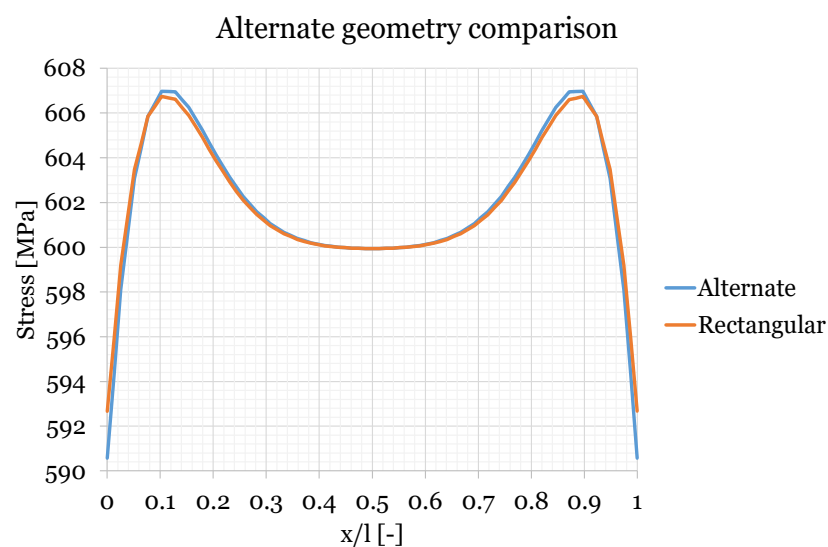


**Figure 4-3:** The stress comparison between the geometry seen in [8] and a rectangular specimen of the same length and roller placement without the radii:  $L_{tot} = 70 \text{ mm}$ ,  $L = 60 \text{ mm}$ ,  $l = 20 \text{ mm}$  & a cross section of  $6 \times 6 \text{ mm}^2$

These results show little to no impact when introducing these radii. The drawback of added manufacturing time and materials does not outweigh the use of intricate designs like these. In this case, the alternate geometry results in a larger peak stress amplitude – albeit a very slight one, not worth the added time and resources needed to manufacture, post process and test this geometry.

#### 4.3.2 Cross section study results

Followingly, the results when varying the specimen breadth and height – while keeping the roller placements constant according to the baseline specimen – are presented below in Figure 4-4.

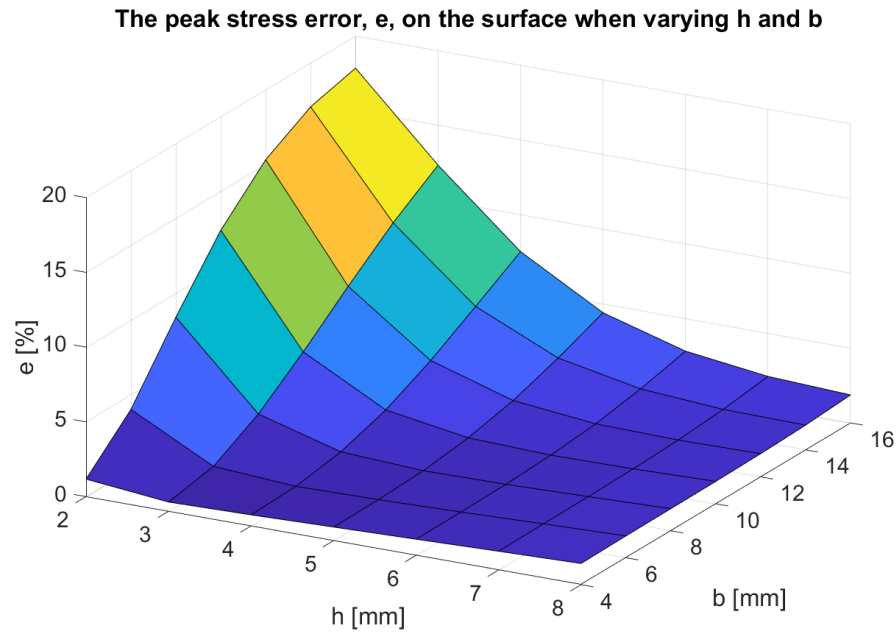


**Figure 4-4:** 3D surface plot of the peak stress error in percentage when varying  $h$  and  $b$  of the baseline specimen with  $L = 80$  mm and  $l = 40$  mm.

When analyzing this plot, a diagonal line going from  $h = 2$  mm &  $b = 16$  mm is prominent. Within this line, the error is kept below 2%, and this provides a limit which should be taken into consideration when designing specimen. This limit shows that  $b$  should be less than  $2h$  for specimen optimization, which can be defined as:  $b < 2h$ . The tensile stress deviation across the test surface for the three limits seen above –  $h = 8$ ,  $b = 4$  &  $b = 2h$  – can be seen in Figure 4-5, -6 & -7. Additionally, the error increases rapidly when the dimensions go beyond this limit.

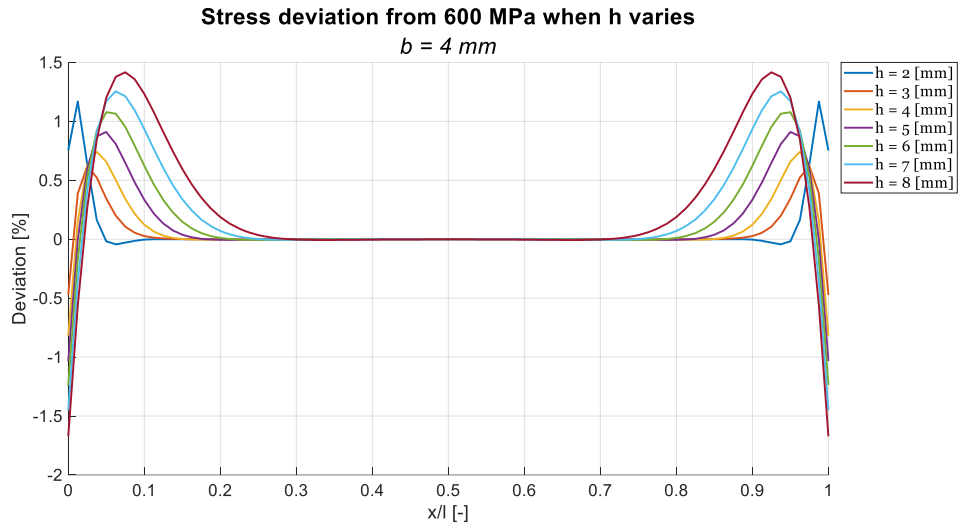


**Figure 4-5:** The resulting stress curve when the height is set to 8 mm and the breadth varies.

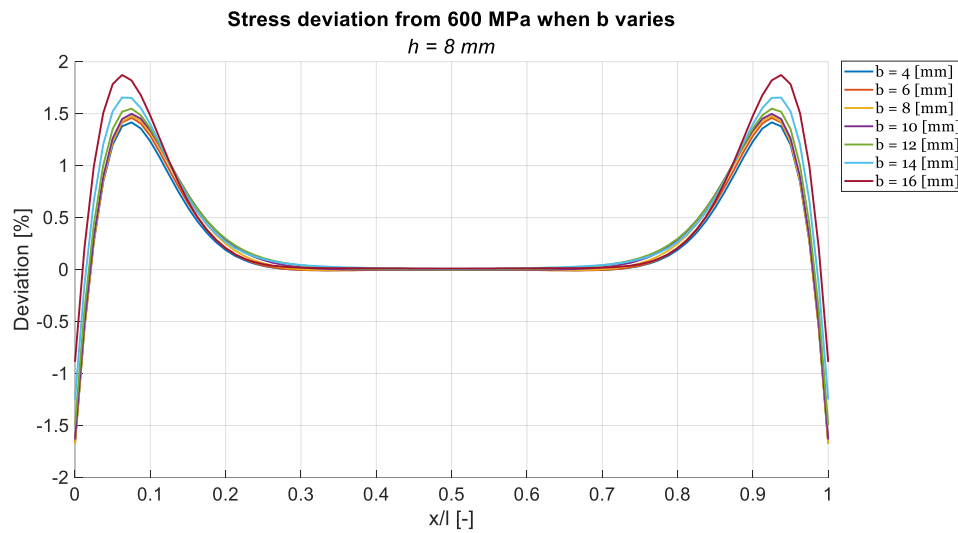


**Figure 4-6:** The resulting stress curves when the height varies and the breadth is set to 4 mm.

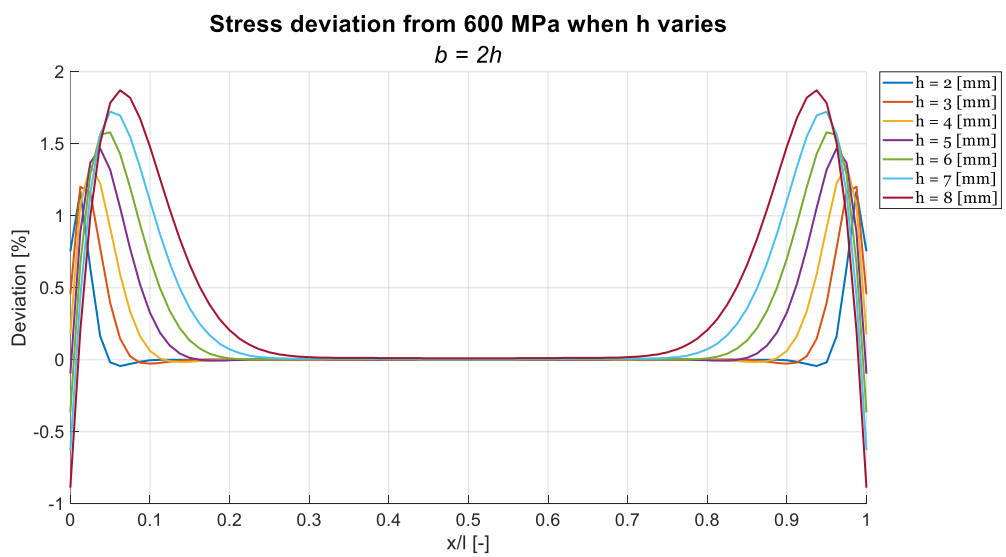


**Figure 4-7:** The stress curve behavior when  $b = 2h$ .

Furthermore, stress behavior is slightly different when approaching the limit and needs to be considered when deciding on specimen geometry. In Figure 4-8 below, the surface stress behavior of thin and wide specimen geometries is shown.

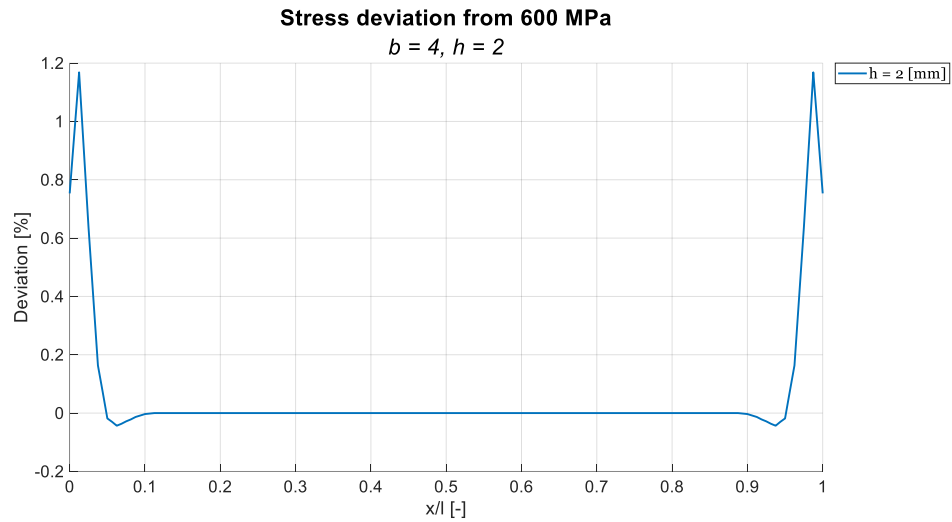


**Figure 4-8:** The stress behavior for thin and wide specimen geometries.

#### 4.3.3 Roller placement study results

The parameter studies showed that one of the major contributors to lowering the peak stresses caused by wedging was the variable named  $\delta$  (Figure 3-14). The result when  $\delta$  and  $L$  varies can be seen in the surface plot below, Figure 4-9, where the error in percentage is plotted against these variables.

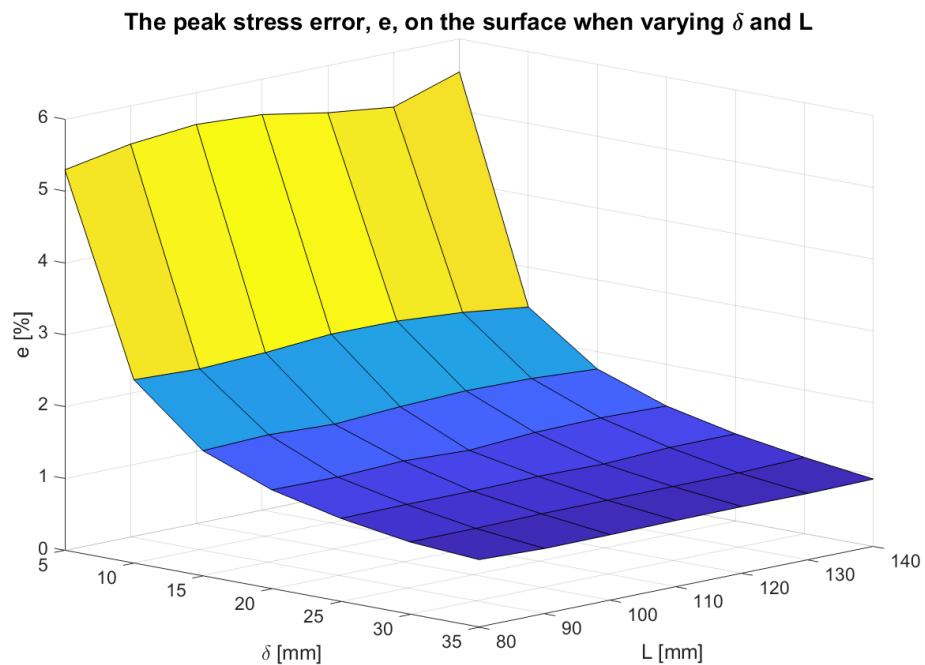


**Figure 4-9:** 3D surface plot that shows how the tensile stress error is dependent on the parameters  $\delta$  and  $L$ .

The error trend shows that a  $\delta$  which is larger than 35 mm will result in wedging peak stresses that deviate less than 1% compared to the nominal stress. Bearing this in mind, the distance between the inner rollers,  $l$ , must still be taken into consideration. Since  $l = 0.2L$  is the criterion for pseudo-3PB behavior, as described in Chapter 3.5.1. In Figure 4-10 below, the surface tensile stress is plotted when  $\delta = 35$  mm and  $L$  vary from 80 to 140 mm.

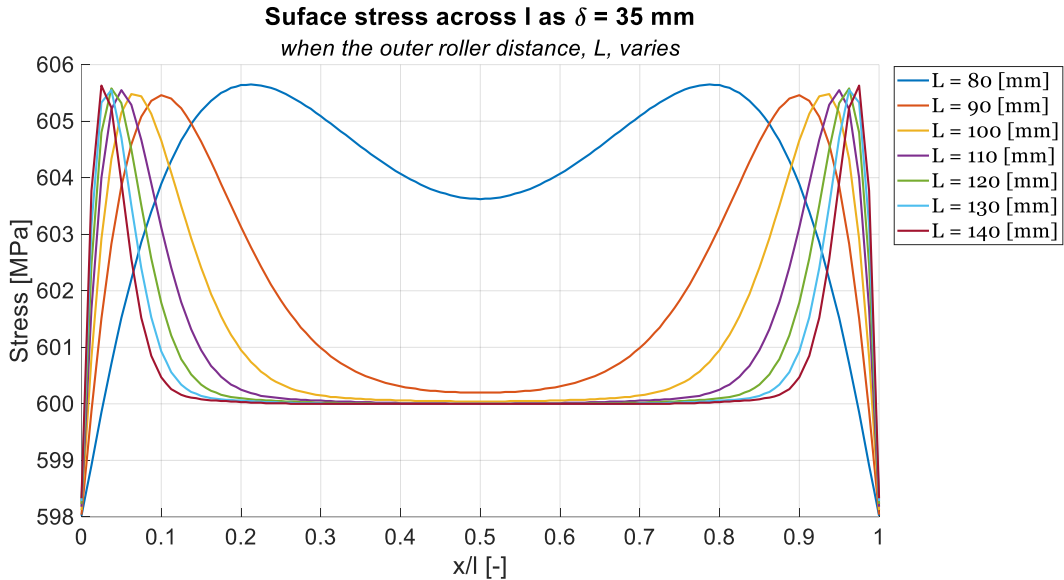


Figure 4-10: The surface stress across  $l$  while varying  $L$  with a constant  $\delta$ .

When  $L = 80$  mm and  $\delta = 35$  mm it leads to  $l = 10$  mm and the resulting surface stress is moving towards a pseudo-3PB behavior. Valid 4PB behavior is seen where  $L \geq 100$  mm which in conjunction with  $\delta = 35$  mm leads to  $l \geq 30$  mm – or in relation to  $L$ :  $l \geq 0.3L$ .

A separate graph where the error is plotted against  $\delta$  can be seen below Figure 4-11, which provides a clear image of how  $\delta$  influences the error.

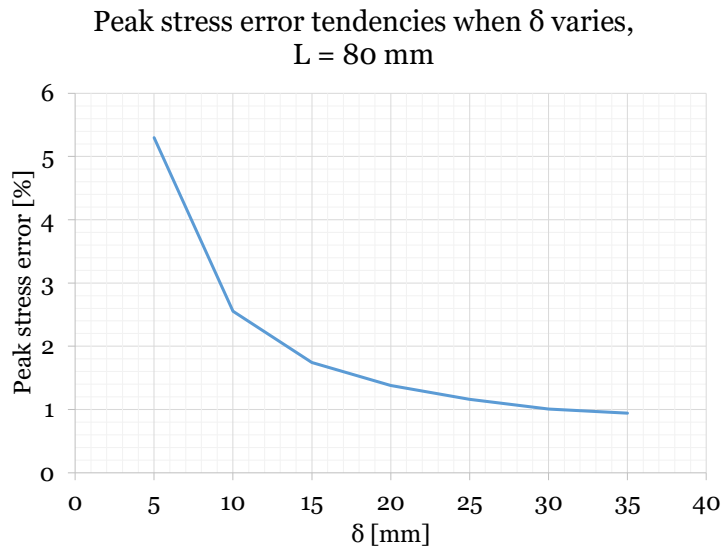


Figure 4-11: The peak stress error plotted against an increasing  $\delta$  when  $L = 80$  mm.

#### 4.4 Error Sensitivity Result

The error sensitivity study results are presented here according to Chapter 3.6.

##### 4.4.1 Eccentric loading results

Eccentrically applied loads have shown to be something 4PB is sensitive to. The resulting peak stress error when the inner rollers are moved from 0 to 1 mm with steps of 0.1 mm – relative to the outer rollers – can be seen below in Figure 4-12. Here the force of each inner roller is  $F/2$  which is the case for GKN Aerospace.

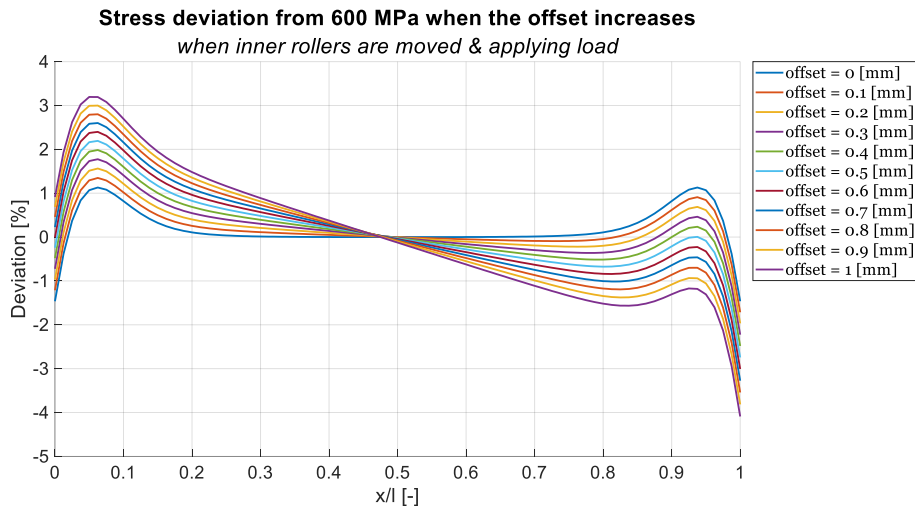


**Figure 4-12:** Tensile stress deviation across the test surface during an increasing eccentric offset when the inner rollers are applying a constant force of  $F/2$  each.

These results behave as expected. The moment arm becomes longer on one side of the inner rollers and shorter on the other, which leads to tensile stress increasing on one side and decreasing on the other. The calculated bending moment and shear forces can be seen in Figure 4-13. Note that this diagram is plotted against an offset of 3 mm: this provides a clearer representation of how the bending moment changes during an eccentric loading scenario. Additionally, the peak stress error was plotted against the offset and can be seen below in Figure 4-14.

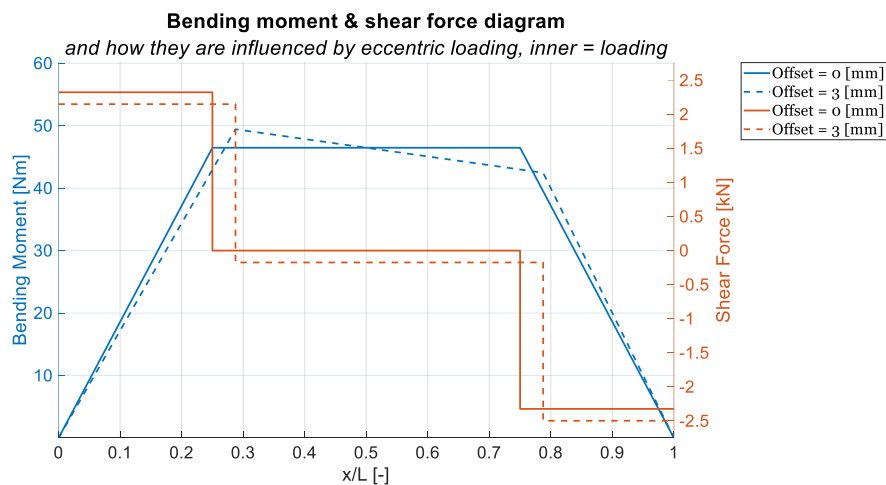


**Figure 4-13:** BMD & SFD comparison during an eccentric offset of 3 mm when inner rollers are applying the load.

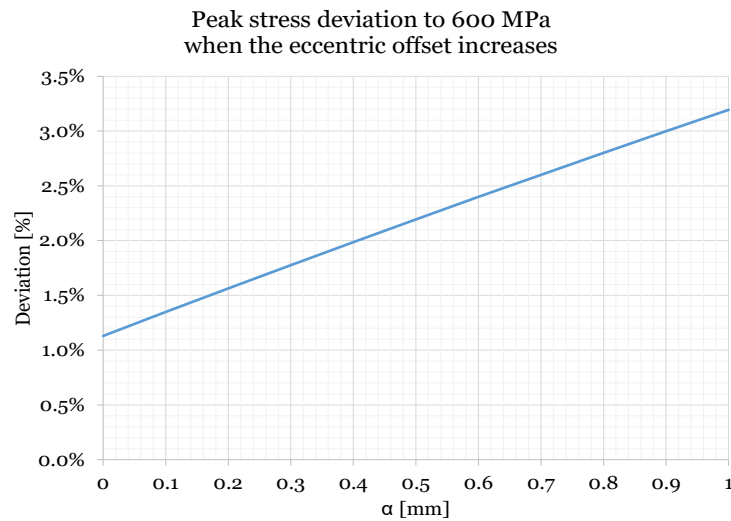


**Figure 4-14:** The peak stress deviation in percentage when the eccentric offset increases.

The result from Chapter 4.3.3 shows that a larger delta tends to lower the error, and therefore, the influence of a larger delta on an eccentric load offset of 1 mm was plotted and is seen in Figure 4-15. This shows that the eccentric loading error is also minimized when delta is as large as possible.

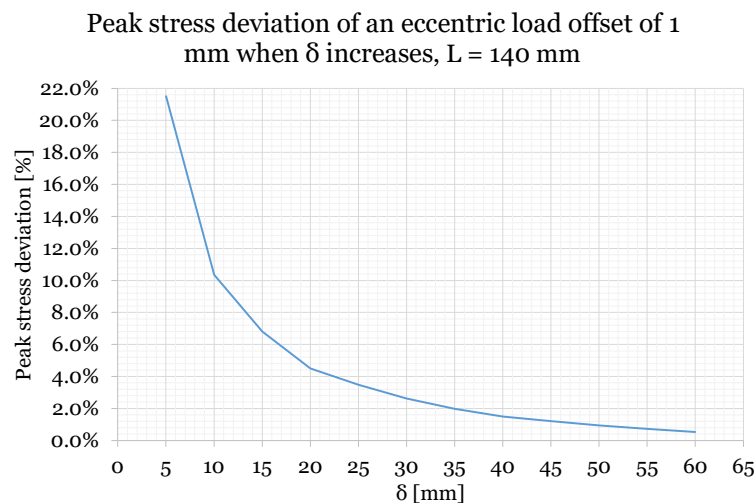


**Figure 4-15:** Peak stress deviation in percentage when an eccentric offset of 1 mm is present, plotted against varying delta.

Further analysis discovered that the behavior of the surface stress is dependent on which rollers are applying the load. When the outer rollers are applying the load, the results are as shown in above figures. In Figure 4-16 & Figure 4-17 below are the corresponding surface stress curves, BMD and SFD when the outer rollers are applying a constant load of  $F/2$  each. Additionally, a comparative plot of the peak stresses of each case can be seen in Figure 4-18. A comparison between the corresponding BMD for each case can be seen in Figure 4-19, plotted for an offset of 3 mm.

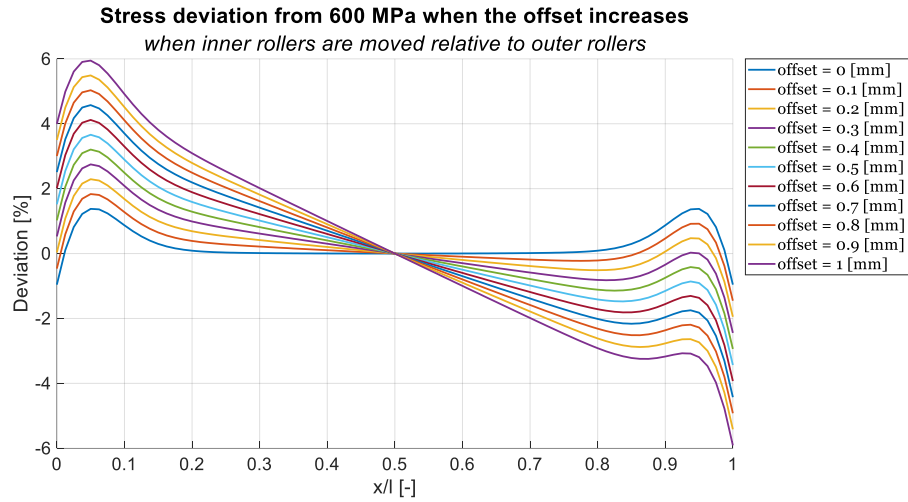


Figure 4-16: The tensile stress deviation when the outer rollers are applying the load during eccentric loading.

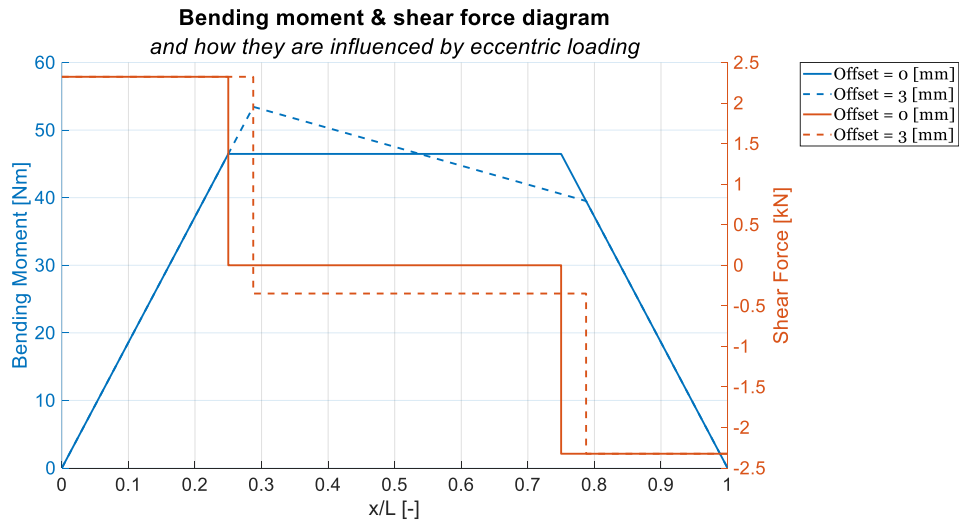


Figure 4-17: BMD & SFD comparison during an eccentric offset of 3 mm when the outer rollers are applying the load.

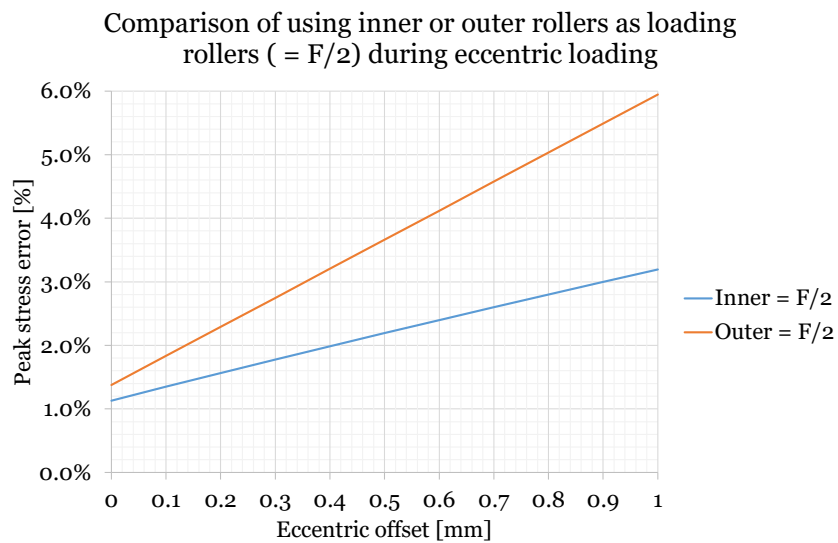
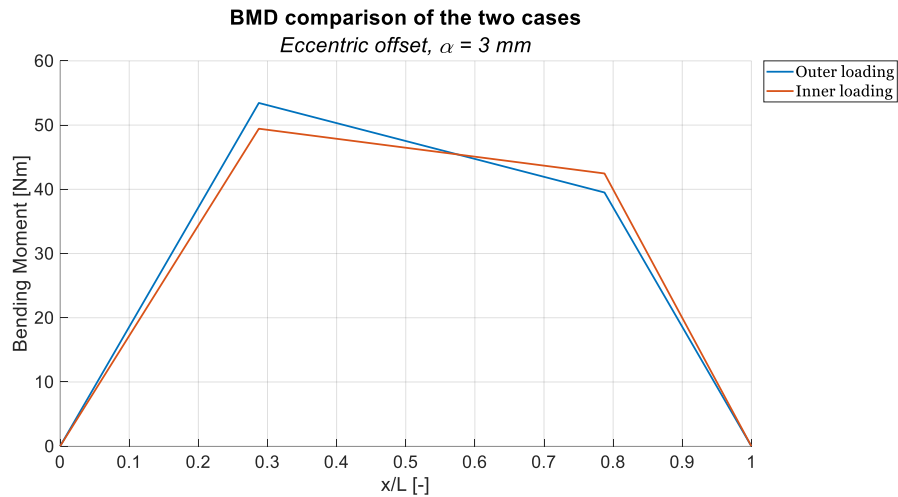
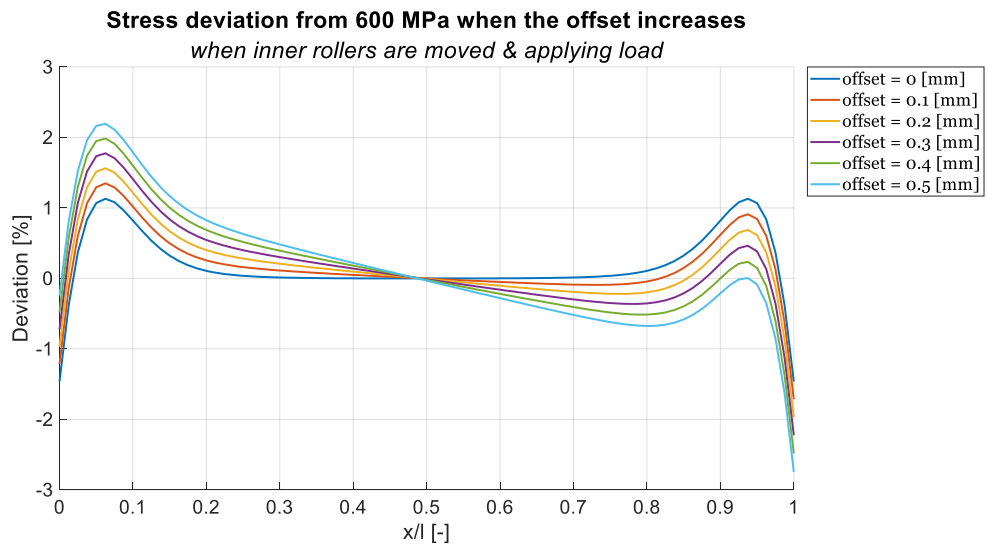


Figure 4-18: The peak stress error in percentage during an increasing eccentric offset for the two different loading cases.



**Figure 4-19:** BMD comparison of the two eccentric load cases when the offset is 3 mm.

These differences are because of the different behaviors of the reaction forces, which are described in the diagrams seen in Chapter 3.6.1. Results when the offset limit of  $\pm 0.5$  mm was implemented in this study can be seen in Figure 4-20 and Figure 4-21 below. At the far end of the limit, the peak stress deviation difference when using inner rollers for applying the load is approximately 1.5% lower – see Figure 4-18. This confirms that 4PB is less sensitive to eccentric loading when the inner rollers are applying a constant load of  $F/2$ .



**Figure 4-20:** Tensile stress deviation across the test surface during an increasing eccentric offset within real limits.

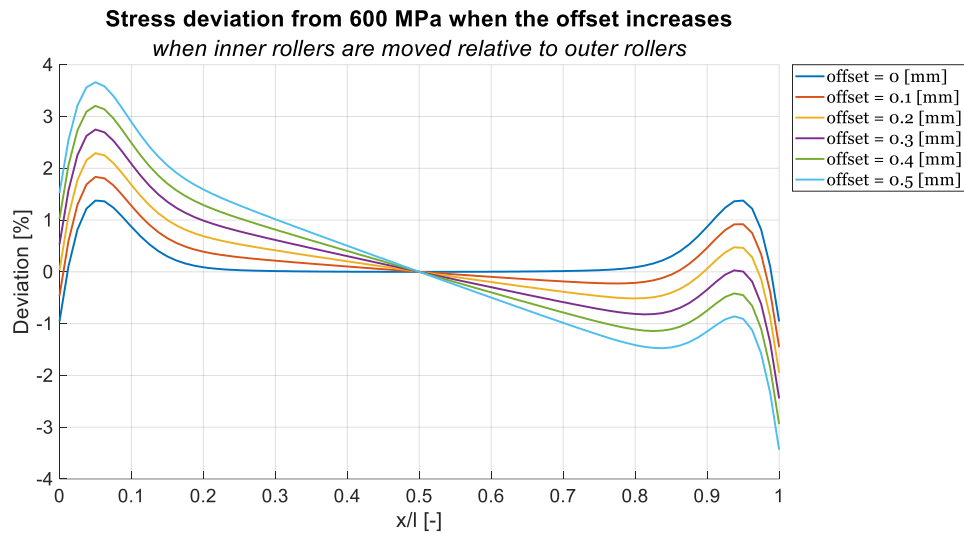


**Figure 4-21:** The tensile stress deviation when the outer rollers are applying the load during eccentric loading, within real limits.

The main takeaway from these results is that eccentric loading completely disrupts the main advantage of 4PB: equal stress along the test surface. This means that results will be invalidated if there is an eccentric offset present. This offset does not have to be large, since unequal stress will be present with a mere 0.1 mm offset. Wedging stress can be minimized by altering the specimen dimensions, however, eccentric loading can only be avoided by making sure that the rollers are aligned and centered with each other and the specimen. Evaluating how this error can be avoided is a crucial part of further developing 4PB.

Furthermore, lowering the wedging stress will decrease the magnitude of the error, and this in turn lowers the overall average stress on the test surface (see Figure 4-14). This indicates that almost equal stress can be achieved by increasing  $\delta$ , which decreases the tensile stress difference along the test surface.

#### 4.4.2 Non-perpendicular loading results

The non-perpendicular loading study found that the peak stress error only depended on the rotation of the inner rollers. This error proved to have a smaller impact on the peak stress error than the eccentric loading error. The peak stress error increase in percentage can be seen plotted against the rotation angle in degrees in Figure 4-22. The biggest contribution this error has made is the introduction of twisting, which probably affects the overall fatigue properties of the specimen by introducing shear forces. The normal stress on the test surface of the specimen when the inner rollers are rotated 5 degrees can be seen in Figure 4-23. The stress surface for the three other cases can be seen in Appendix D.

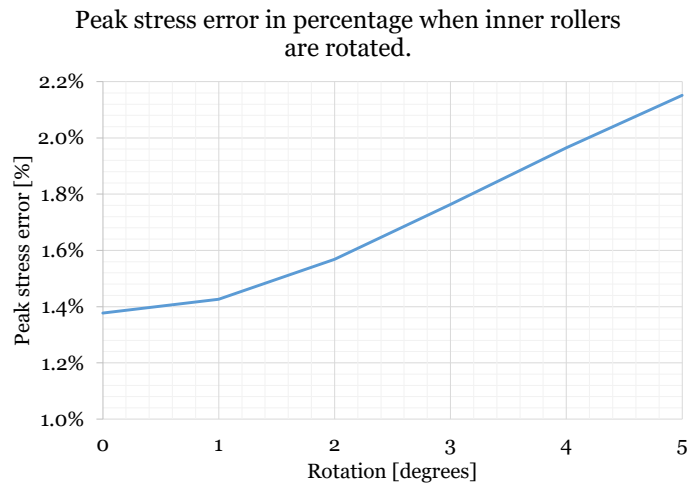


Figure 4-22: Peak stress error when the inner rollers are rotated.



Figure 4-23: The normal stress surface profile of the specimen when the inner rollers are rotated 5 degrees

Further discussion with the laboratory personnel revealed that this degree of rotation is larger than what is expected from the current setup: the maximum rotation was calculated to be approximately 0.5 degrees. This calculation was performed by assuming that the top carrier part of the rig moved a maximum of 0.8 mm at each end, see Figure 4-24. Looking at the graph in Figure 4-22 the peak stress is almost 2.2% at a rotation of 5 degrees, which intuitively concludes that 4PB is less sensitive to rotation of the inner rollers than to eccentric loading. Additionally, if it is possible to keep the rollers within 0.5 degrees of rotation the peak stress would barely be impacted.

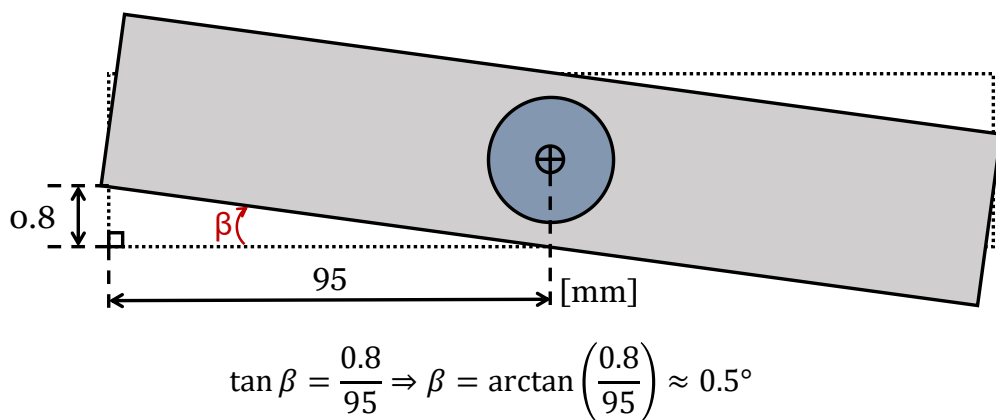


Figure 4-24: Top view of the upper part of the 4PB test rig, rotated to show how the maximum rotation was calculated. The dotted outline is the ideal, or starting, position of the carrier.

## 4.5 Discussion

This thesis project has been equal parts challenging and interesting. In the beginning, it was thought to simply validate the results seen in the Oxford article [4] but these results could not be replicated no matter how the model was altered. It is still unclear what caused these result deviations. What continued was a project which proved that wedging stresses are not as severe as they were thought to be. In fact, the specimen used by GKN Aerospace showed to be within an acceptable error range. The peak stress for the baseline specimen was shown to be less than 2% larger than the nominal stress, and since the total error limit was set to 5% there is a margin of more than 3% for the other error sources.

Additionally, the total error can be kept below 5% by keeping the eccentric offset below 0.8 mm and the rotation of the inner rollers within 5 degrees. Since discussion with the laboratory personnel showed that the worst eccentric offset is 0.5 mm and rotation of the inner rollers less than 1 degree, the biggest error – based on the findings of this project – is less than 4%. The error can be further lowered by keeping  $\delta$  as large as possible, setting the inner roller distance  $l \geq 0.3L$  and keeping the breadth  $b < 2h$ . Which makes sense: Euler Bernoulli beam theory is based on long and slim beams. The longer and slimmer the specimen is, the more it is going to coincide with the theory.

The given limits of the 4PB test setup are important to keep in mind when looking at the specimen design. For example, a specimen could have the following measurements:  $200 \times 30 \times 3 \times 4 = L \times l \times b \times h$  which would result in peak stresses less than 1% larger than nominal stress and still be compliant with the dimension limits. The applied load, however, would become 113 N, which is outside of the limit set by GKN (Table 3-4). The specimen would also be inconvenient when it comes to manufacturing it, preparing it and setting it up for 4PB testing. Specimen design can therefore not solely be based on lowering peak stress. Furthermore, an unexpected finding which lowers the sensitivity to eccentric loading is using the inner rollers as the load applying rollers, as is the case for GKN Aerospace.

There are more error sources that impact the validity of 4PB [6] than the ones that have been evaluated in this thesis project. The sooner more of these errors are investigated the better. However, the findings of this thesis project provide good guidelines for designing specimen geometry to minimize these studied errors. Continuing, the non-perpendicular loading phenomenon could benefit from being studied further, perhaps with a more complex model to find out how the introduction of twisting influences fatigue properties.

The purpose of this thesis project was to deepen the understanding and evaluate the validity of four-point bending. I believe that this has been achieved, even if there is still work to be done. Further evaluating error sources and looking into more complex simulations should probably be the next step in 4PB research. The project as it stands is a good baseline for what should be included in a future international standard. Geometry specifications give insight into how to minimize the wedging stresses, which has also been proven to be less severe than once thought. Which by itself lowers uncertainties of 4PB, for example if the initiated cracks are due to the surface roughness or localized stress peaks. Since a larger testing surface is essential when looking into how AM surfaces affect fatigue properties, it was a relief when it was proven that it is possible to have a larger surface while still minimizing peak stress error. The total error can also be kept within  $\pm 5\%$ , which is a good guideline for fatigue testing.

Overall, this thesis project has provided the mechanical testing sector with valuable insight into how 4PB works and its validity. A standard within four-point bending is not entirely out of reach, with further research based on this work it will not be long for a more complete guide.



## 5 Conclusions and Future Work

The conclusions that were drawn during the thesis project, what limitations were met and recommended future work to further evaluate the 4PB method.

### 5.1 Conclusions

The 4PB testing method has proven to be a method which requires further investigation to clear the uncertainties. During the process of this thesis project, the wedging stress phenomenon has been revealed to not be as severe as it was perceived before due to the results presented by [4]. Which has been proven by the model evaluation in Chapter 3.2 and the results presented in Chapter 4.1.

With an optimized geometry, these localized stress peaks can be kept below a 1% deviation of the specified nominal stress, although the setup limits must be taken into consideration. The optimal specimen geometry is specified by the following relations seen in Table 5-1:

**Table 5-1: Optimal relations for the dimensions of 4PB specimen to lower peak stresses.**

Relation	Variables	Limit	Notes
Inner and outer rollers	$\delta$	$\delta \rightarrow \infty$	$\delta$ needs to be as large as possible.
Inner roller distance	$l$	$l \geq 0.3L$	Pseudo-3PB is seen when $l$ approaches lengths smaller than this limit.
Height and breadth	$h, b$	$b < 2h$	-

When moving outside of these limits, the wedging peak stresses increase rapidly. This is especially true for thin and wide specimen. Additionally, the peak magnitude is also directly dependent on  $\delta$ : when  $\delta \geq 35 \text{ mm}$  the peak stress can be kept below 1% larger than nominal.

Furthermore, 4PB is sensitive to eccentric loading. An eccentric offset of 1 mm is enough for the peak stress to reach magnitudes approximately 3% larger than nominal stress when the inner rollers are applying the load. This concludes that only a slight offset is needed for the peak stress to increase, and it is therefore important to take necessary action to prevent this error from occurring. One option is to use plastic guides which in theory should minimize the movement of the inner rollers to  $\pm 0.5 \text{ mm}$ . Consequently, it is also better to use the inner rollers as loading rollers since this lowers the peak stress error significantly. An error source which 4PB appears to be less sensitive to is non-perpendicular loading. At a 5-degree angle, the peak stress increases by approximately 0.75%, which would lead to a peak stress error slightly larger than 2%.

### 5.2 Limitations

The major limitation of this project has been the time-consuming simulations, performing large parameter studies takes time and it limits the amount of work which can be done. Specifically, it was not possible to work on other simulations due to computer limitations. Other aspects of the project were performed while simulations were running, like altering the MATLAB code, performing hand calculations or working on the report.

Additionally, lack of experience with Ansys proved to be a limitation. It made it more difficult to get started with the simulations, but this improved significantly in the second half of the project.

The overall lack of research regarding 4PB, specifically applied to metal components, proved difficult, and why there are few specific comparisons regarding specimen geometry.

### 5.3 Future Work

This project managed to investigate the basics of four-point bending, as well as possible sources of error other than wedging stresses – and the sensitivity to these. To further evaluate the process of 4PB, the findings and processes of this project can be implemented into machine learning software or an Artificial Neural Network, for example Orange Data Mining. This would make it possible to extend the search for optimal geometry by performing more in-depth simulations and analyses.

Furthermore, it would be wise to look at other sources of error, unevenly applied force on specimen surface is one of these. In this project, the line force applied by the rollers was assumed to be even along the breadth of the specimen, but what would happen if this force was unevenly spread along the line of contact? What would happen if one roller applied more load than the other?

Roller deformation and movement is another aspect which would be valuable to investigate. Implementing surface roughness into the model could also be implemented together with applying a cyclic load which would allow for an even more realistic FEA simulation model.

This as well as further analysis of fatigue properties could be investigated by creating a more complex and in-depth simulation model. Implementing roller models and surfaces interactions and performing cyclic load scenarios would give a deeper understanding of 4PB for example.

Additionally, more geometry variations might be interesting to investigate, even if it was concluded that this introduces complexity in manufacturing, there might exist a geometry which outweighs the negative impacts of its complexity.

Ultimately, it would be beneficial to perform real-world four-point bending tests to further evaluate the error sensitivity studies. This could be performed by, for example, applying an eccentric load with predetermined offsets. More measurements should also be taken to capture the wedging stresses which could further validate simulation models like this one.

### 5.4 Reflections

What this thesis has concluded is that wedging stresses are present in all convenient specimen geometries, they cannot be diminished by altering the geometry to something more complex. This means that simple geometries like rectangular blocks can be used for 4PB testing. Using geometries like these can limit the material waste, time and resources. The same is true for post processing, which is easier for rectangular specimen. This will not only lower the environmental impact but also the economic impact on GKN Aerospace and other industries utilizing four-point bending.

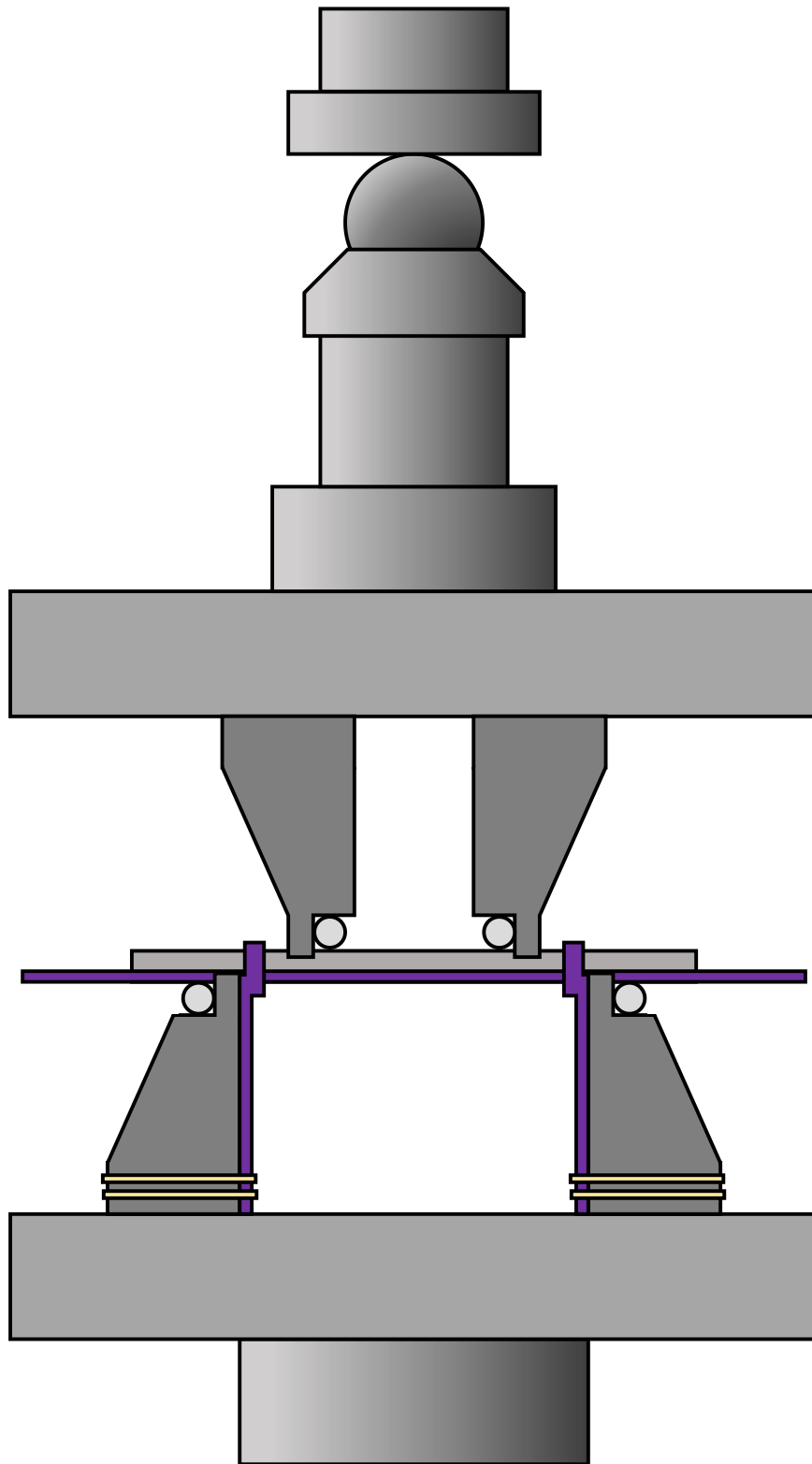
Furthermore, this thesis creates a possible base for an international standard which would improve communication between different parties using this method, which would improve the overall 4PB process and ultimately help create safer products, which is crucial in the aerospace industry.

## References

- [1] A. Knoeppel, "IMTS," 24 September 2025. [Online]. Available: <https://www.imts.com/read/article-details/Additive-Manufacturing-in-Aerospace-Applications-Materials-Trends/2163/type/Read/1>. [Accessed 16 February 2026].
- [2] "www.gknaerospace.com," GKN Aerospace, [Online]. Available: <https://www.gknaerospace.com/innovation/additive-manufacturing/>. [Accessed 16 January 2026].
- [3] N. Sanaei and A. Fatemim, "Analysis of the effect of surface roughness on fatigue performance of powder bed fusion additive manufactured metals," *Theoretical and Applied Fracture Mechanics*, vol. 108, 2020.
- [4] T. Zhai, Y. Xu, J. Martin, A. Wilkinson and G. Briggs, "A self-aligning four-point bend testing rig and sample geometry effect in four-point bend fatigue," *International Journal of Fatigue*.
- [5] G. D. Quinn and R. Morrell, "Design Data for Engineering Ceramics: A Review of the Flexure Test," *Journal of the American Ceramic Society*, vol. 74, no. 9, pp. 2037-2066, 1991.
- [6] G. D. Quinn, B. T. Sparenberg, P. Koshy, L. K. Ives, S. Jahanmir and D. D. Arola, "Flexural Strength of Ceramic and Glass Rods," *Journal of Testing and Evaluation*, vol. 37, no. 3, pp. 222-244, 2009.
- [7] T. Lube, M. Manner and R. Danzer, "The miniaturisation of the 4-point-bend test," *Fatigue & Fracture of Engineering Materials & Structures*, vol. 20, no. 11, pp. 1605-1616, 1997.
- [8] S. Romano, E. Peradotto, S. Beretta, D. Ugues, L. Barricelli, G. Maculotti and L. Patriarca, "Fatigue strength estimation of net-shape L-PBF Co-Cr-Mo alloy via non-destructive surface measurements," *International Journal of Fatigue*, vol. 178, 2024.
- [9] "www.twi-global.com," The Welding Institute, [Online]. Available: <https://www.twi-global.com/technical-knowledge/faqs/what-is-mechanical-testing>. [Accessed 16 January 2026].
- [10] "nl-test.com," NL Scientific, [Online]. Available: <https://nl-test.com/news/flexural-testing>. [Accessed 16 February 2026].
- [11] Erika, "Updated lab setup for four point bending, VOLS: 10320040," GKN Internal Document, Trollhättan, 2025.
- [12] Z. Chen, J. J. Moverare, R. L. Peng, S. Johansson and D. Gustafsson, "On the conjoint influence of broaching and heat treatment on bending fatigue behavior of Inconel 718," *Materials Science and Engineering*, vol. 671, pp. 158-169, 2016.

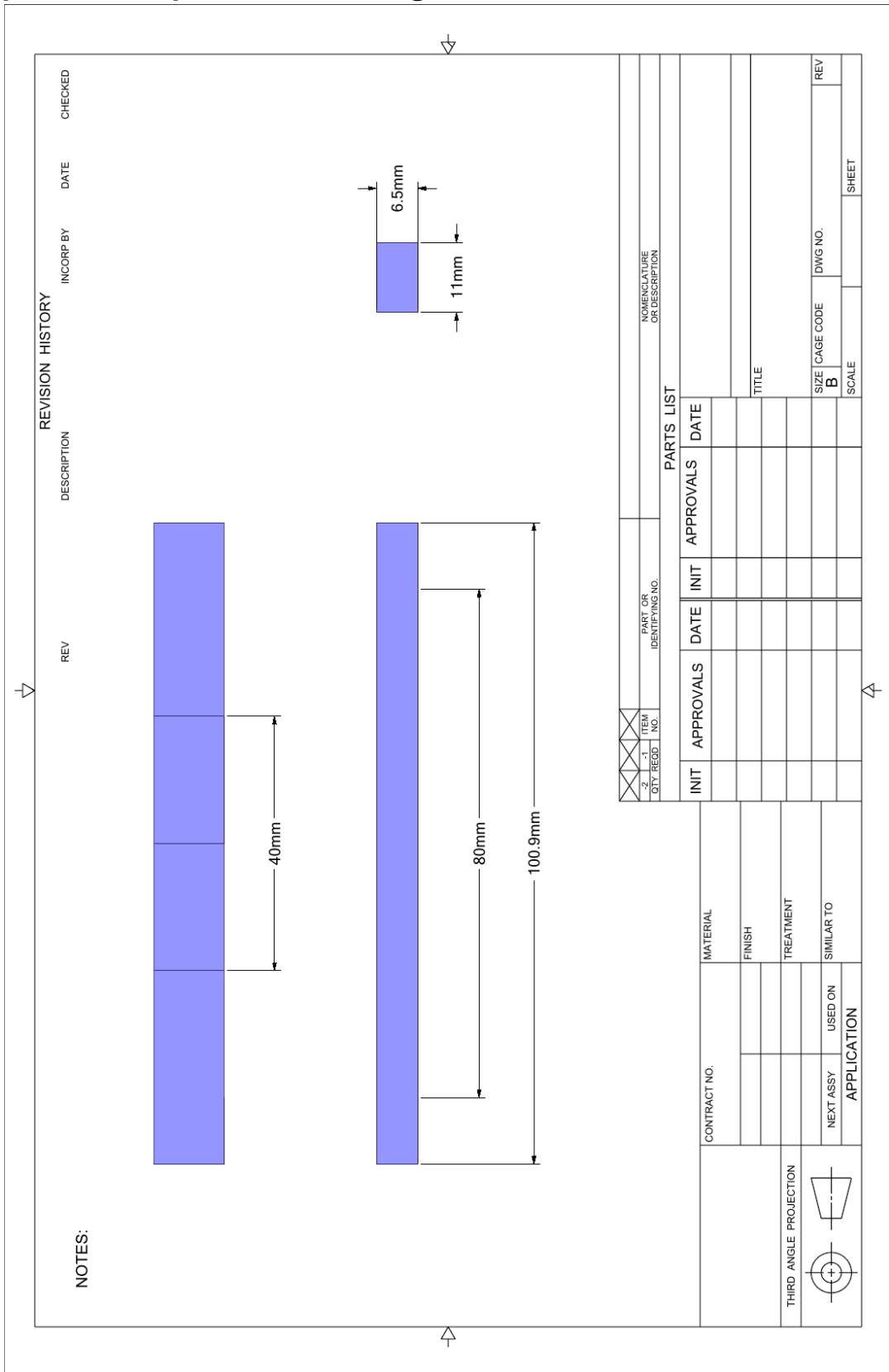


## Appendix A: 4PB Test Rig at GKN Aerospace



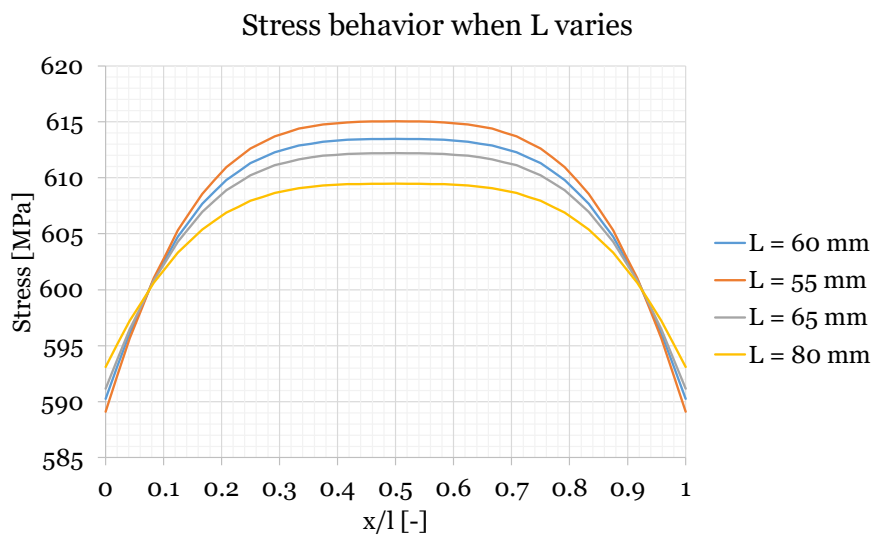
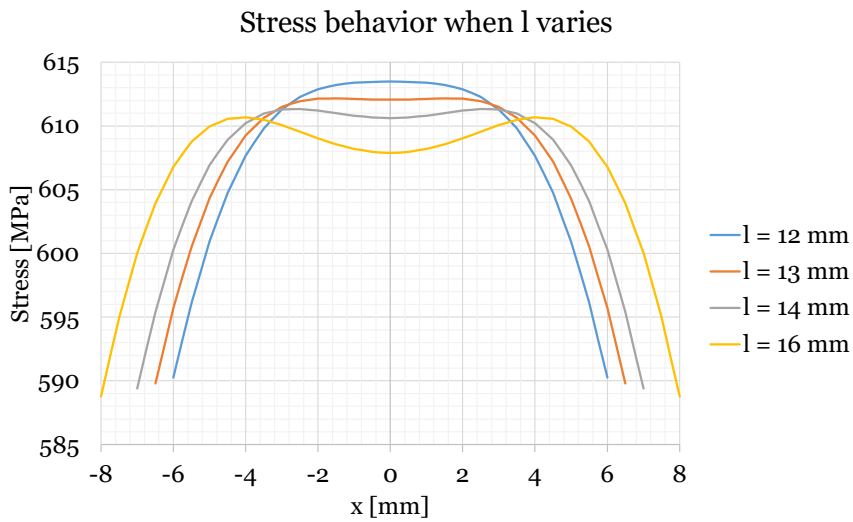
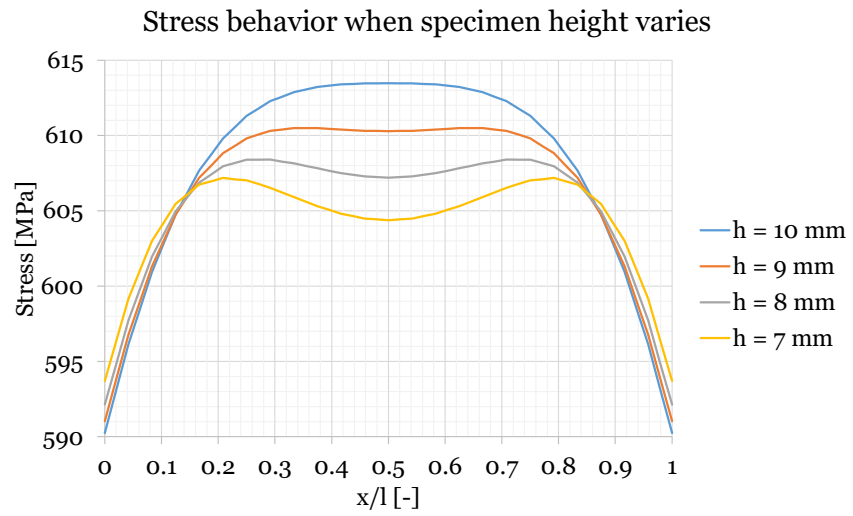
Appendix A: Simplified diagram of the 4PB test rig at GKN Aerospace. Purple components are the plastic spacers used to align the specimen.

## Appendix B: Specimen Drawing



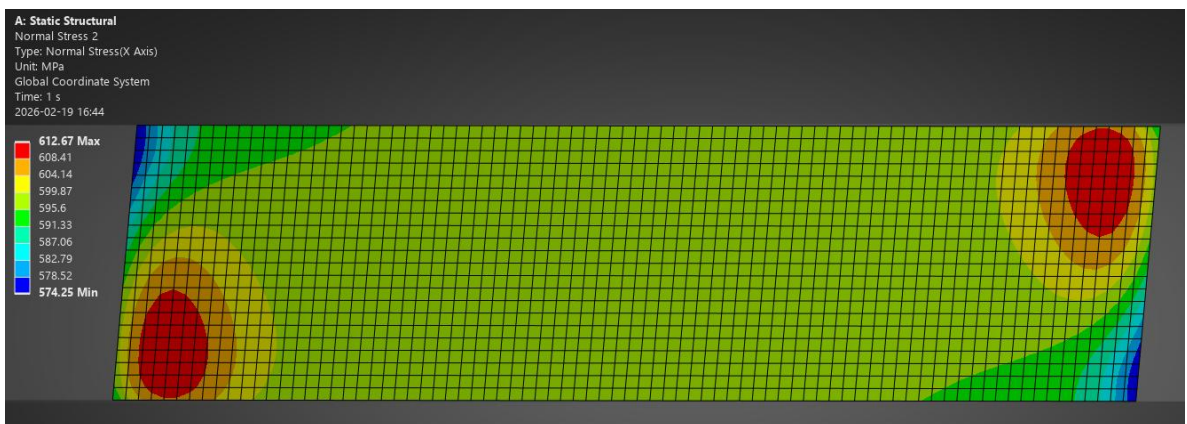
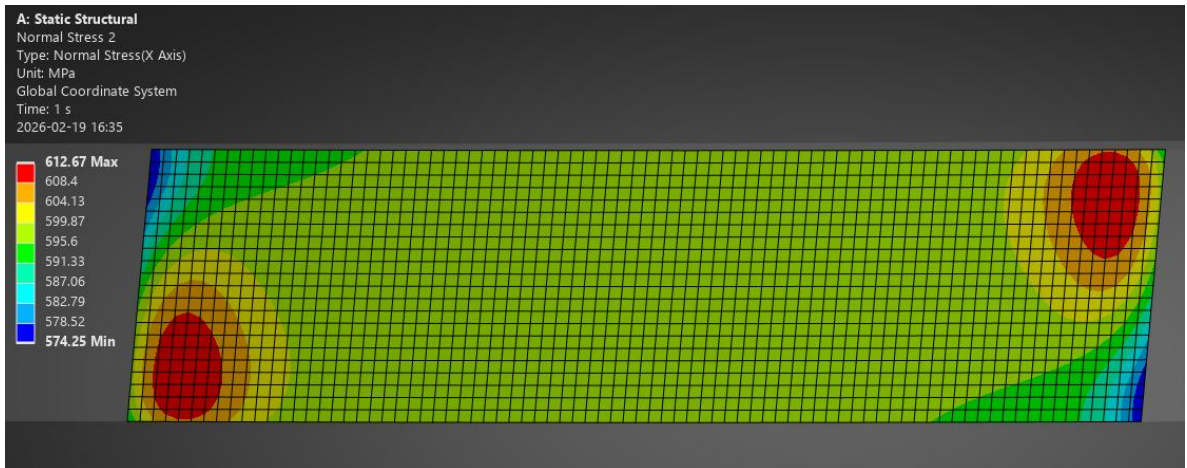
Appendix B: Drawing of the current specimen at GKN Aerospace which was used in the micro strain gauge calibration measurements.

## Appendix C: Geometry Study of a Proposed Ideal Specimen



Appendix C: The geometry study results when investigating the proposed ideal specimen dimensions.

## Appendix D: Non-Perpendicular Loading Surfaces



**Appendix D:** The 3 other cases of non-perpendicular loading from top to bottom: outer rollers rotated 5 degrees, both sets of rollers rotated 5 degrees in the same direction and finally rotated 5 degrees in the opposite direction.